

VVV SURVEY OF BLUE HORIZONTAL-BRANCH STARS IN THE BULGE-HALO TRANSITION REGION OF THE MILKY WAY

KATHERINE MONTENEGRO,^{1,2} DANTE MINNITI,^{1,2,3} JAVIER ALONSO-GARCÍA,^{4,2} MAREN HEMPEL,⁵ ROBERTO K. SAITO,⁶
TIMOTHY C. BEERS,⁷ AND DAVID BROWN³

¹*Departamento de Ciencias Físicas, Facultad de Ciencias Exactas, Universidad Andrés Bello, Av. Fernández Concha 700, Las Condes, Santiago, Chile.*

²*Instituto Milenio de Astrofísica, Santiago, Chile.*

³*Vatican Observatory, V-00120 Città del Vaticano, Vatican City State, Europe.*

⁴*Unidad de Astronomía, Facultad de Cs. Básicas, Universidad de Antofagasta, Av. U. de Antofagasta 02800, Antofagasta, Chile.*

⁵*Instituto de Astrofísica, Pontificia Universidad Católica de Chile, Av. Vicuña Mackenna 4860, Santiago, Chile.*

⁶*Departamento de Física, Universidade Federal de Santa Catarina, Trindade 88040-900, Florianópolis, SC, Brazil.*

⁷*Department of Physics and JINA Center for the Evolution of the Elements, University of Notre Dame, Notre Dame, IN 46556, USA.*

(Accepted 2018 September 19)

Submitted to ApJ

ABSTRACT

We characterize the population of blue horizontal-branch (BHB) stars in the bulge-halo transition region of the Milky Way using the VISTA Variables in the Vía Láctea (VVV) ESO Public Survey data. The selection of BHB stars is made using the globular cluster M22 as a reference standard, and constructing color-magnitude and color-color diagrams with specific cuts in the $ZYJHK_s$ near-infrared (IR) passbands. A total of 12,554 BHB stars were detected, in a region within $-10.0^\circ \leq \ell \leq 10.2^\circ$ and $-10.2^\circ \leq b \leq -8.0^\circ$. We provide accurate coordinates and near-IR photometry for this sample of BHB stars. We searched for over-densities of stars with sizes similar to those of known globular clusters and stellar streams. By comparing real data with Monte Carlo simulations, we conclude that the few over-densities detected are of low significance. We also constructed K_s -band light curves for the BHB stars to study their variability. Taking an average of 52 epochs to calculate periods and amplitudes, we identify hundreds of candidate eclipsing binaries and a dozen pulsating stars. Finally, we made some comparisons with results obtained in a previous study for RR Lyrae variable stars in this same region.

Keywords: Galaxy: bulge — stars: horizontal-branch — stars: binaries: eclipsing

1. INTRODUCTION

The VISTA Variables in the Vía Láctea (VVV) is an ESO Public Survey that is targeting the central parts of the Galaxy, covering an area of ~ 540 square degrees (Minniti et al. 2010). Its main goal is to study our galaxy’s bulge and southern disk, in order to reveal the corresponding 3D structure through variable stars. VVV combines high-resolution ($\sim 0.34''$ pixel⁻¹), deep ($K_s \gtrsim 18$ mag), near-IR photometry in five bands ($ZYJHK_s$), thus alleviating the problem of high interstellar dust extinction and better resolving the high stellar density regions, allowing us to unveil the stellar populations in this complex area (Saito et al. 2012b). In addition, multi-epoch observations allow us to construct K_s -band light curves to study different variable stars,

enabling the construction of a 3D map of the surveyed region (Gran et al. 2016).

Old metal-poor stars, e.g., RR Lyrae and blue horizontal-branch (BHB) stars, are ideal for tracing old regions of the Milky Way (> 5 Gyr) and constructing their associated number-density maps. They are also very good standard candles, which enable accurate determination of their distances (Clewley & Jarvis 2006). However, BHB stars are ~ 10 times more numerous than RR Lyrae stars. Considering these advantages, as well as the accuracy and depth of the photometric data obtained by the VVV Survey, we can use BHB stars to study the (expected) most ancient part of the Galaxy, such as the bulge-halo transition region. We define this region loosely, at projected Galactocentric distances $1 \text{ kpc} < R_G < 2 \text{ kpc}$. This very special place contains

precious information about the assembly history of the Milky Way.

In the Hertzsprung-Russell color-magnitude diagrams (CMDs) of globular clusters, the horizontal branch is populated by stars which have evolved past the main sequence and red giant branch stage. Such stars are now burning helium in their cores and hydrogen in shells outside the core (Ruhland et al. 2011). Amongst these HB stars, RR Lyrae are found in the instability strip of the horizontal branch, and BHB stars are found to the left of (bluer than) the RR Lyrae along the HB. BHB stars are old, metal-poor Population II objects, found in both globular clusters and in the Galactic halo. Their masses are typically within the range of $0.5M_{\odot} - 1.0M_{\odot}$. They are a very useful tool to trace the Milky Way’s structure, due to their intrinsic brightness and distinctive colors, as well as being readily identifiable because of their spectral features, e.g., a strong Balmer jump, their strong and deep Balmer lines (narrower than main-sequence A-type stars, and deeper than, e.g., subdwarf B-type stars), and their lack of strong metallic features/lines (Smith et al. 2010).

BHB stars in the halo and thick-disk systems of the Galaxy have been studied for decades. Early catalogs (Pier 1982, and references therein; Beers et al. 1988, 1996, 2007; Christlieb et al. 2005), based primarily on identification from objective-prism surveys, have been used to constrain the kinematics of the halo and metal-weak thick disk of the Galaxy (e.g., Thom et al. 2005; Brown et al. 2008; Sommer-Larsen et al. 1997), and provided the first identification of a likely age gradient in the halo of the Milky Way (Preston et al. 1991). Later, much larger catalogs of spectroscopically-confirmed BHB stars from the Sloan Digital Sky Survey (SDSS, York et al. 2000; Yanny et al. 2009) were used to study the rotation curve and mass of the Galaxy out to 60 kpc (Xue et al. 2008), and to explore the age structure of the halo (Santucci et al. 2015). Some 130,000 photometrically selected BHB candidates from SDSS were used by Carollo et al. (2016) to obtain the first accurate estimate of the age gradient in the Galactic halo based on field stars, and to confirm the existence of a so-called “ancient chronographic sphere” of old stars in the halo (first suggested by Santucci et al. 2015), extending from immediately outside the bulge, past the solar vicinity, out to ~ 15 kpc from the Galactic center. Due to the selection criteria employed in the above-mentioned studies, none of these samples extended into the bulge region.

Bulge BHB stars have also been studied in the past, both photometrically and spectroscopically (e.g., Peterson et al. 2001; Zoccali et al. 2003; Terndrup et al.

2004; Busso et al. 2005; Koch et al. 2016), firmly establishing that the Galactic bulge, in spite of being predominantly metal-rich, still contains old and metal-poor BHB stars. However, these previous studies were limited to a relative handful of stars. One of the goals of the present work is to assemble a massive catalog of bulge BHB stars, complementing the existing halo- and disk-system catalogs, in order to enable a suite of follow-up studies. Therefore, in this paper we make a census of these old BHB stars in the bulge-halo transition region, using the VVV near-IR data. We also use this new catalog to search for new globular clusters, and for variable stars such as eclipsing binaries and RR Lyrae.

2. THE VVV DATA

2.1. Observations

The VVV is a public near-IR survey of the inner Milky Way using the $ZYJHK_s$ passbands (Minuti et al. 2010; Catelan et al. 2011b; Saito et al. 2012a), whose coordinates have sub-arcsecond accuracy (Smith et al. 2017), a necessary requirement in this high stellar-density region. The VVV observations were taken with the near-IR camera VIRCAM at the Visible and Infrared Survey Telescope for Astronomy (VISTA) located at ESO Cerro Paranal Observatory (Emerson & Sutherland 2010). VISTA is a 4-m telescope that has been optimized for the near-IR. The VISTA Infrared Camera (VIRCAM) has 16 near-IR detectors with a scale of $0.34''/\text{pixel}$, arranged in a 4×4 pattern with significant gaps between them. The observing sequence consists of 6 individual exposures, spatially shifted in an mosaic pattern, and later combined into a single image, which we refer to as a “tile”. Each tile covers approximately 1.1×1.5 square degrees on the sky. The VVV bulge observations comprise 196 tiles in total, covering a 307 square degree field of view, within $-10.0^\circ \leq \ell \leq 10.2^\circ$, and $-10.2^\circ \leq b \leq 5.0^\circ$. Figure 1 shows a schematic of the bulge region observed by the VVV survey.

The observations are made using the $ZYJHK_s$ filters, and consist of two epochs in $ZYJH$, taken at the beginning and the end of the survey, in years 2010 and 2015, respectively, plus multiple epochs in the K_s -band. The K_s -band variability campaign was carried out between 2010 and 2016, obtaining a total of about 75 observations per field in the VVV bulge area.

The data reduction, calibration, and aperture photometry were carried out by the Cambridge Astronomical Survey Unit (CASU; Irwin et al. 2004). The CASU photometry is tied to the 2MASS system (Cutri et al. 2003; Hodgkin et al. 2009), and is made publicly available at the VISTA Science Archive (VSA, Hambly et al. 2004; Cross et al. 2009). In addition, we have per-

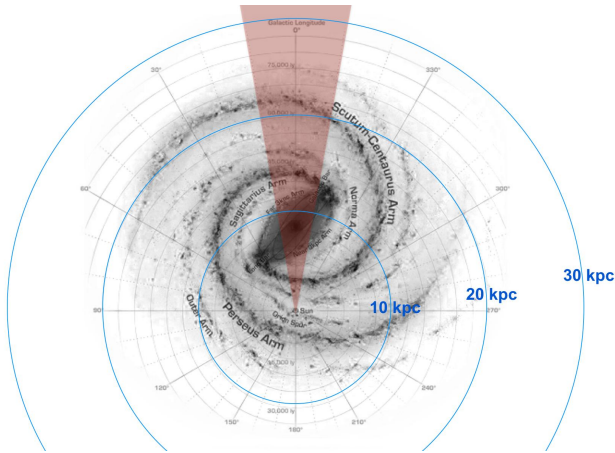


Figure 1. Artistic representation of the Milky Way, seen face-on, based on the Spitzer satellite data (Credits: R. Hurt/Spitzer Space Observatory/NASA). Each concentric circle indicates the distance to the Sun. The shaded region corresponds to the area covered by the VVV survey used in this study.

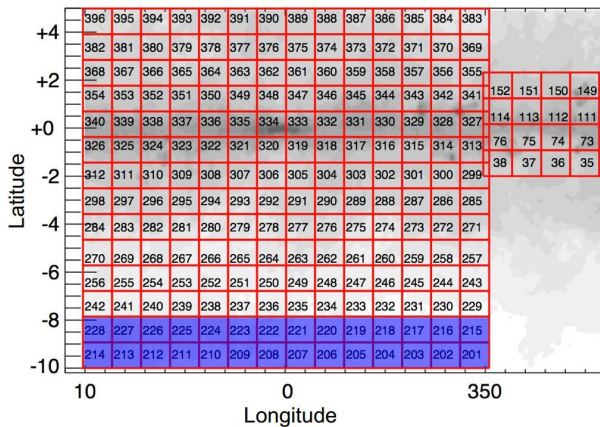


Figure 2. VVV Bulge area in Galactic coordinates (measured in degrees). Tiles used in this work (b201-b228) are colored in blue, and are located in the bulge-halo transition region of the Milky Way.

formed single-epoch PSF photometry in the $ZYJHK_s$ bands for the entire VVV bulge dataset using DoPhot (Alonso-García et al. 2015), in order to obtain deeper and more accurate photometry, adequate for the selection of BHB stars. In this work we analyze the outermost southern VVV bulge tiles, from b201 to b228 (Figure 2), covering an area within $10.0^\circ \leq \ell \leq 10.2^\circ$, and $-10.2^\circ \leq b \leq -8.0^\circ$, for a total of about 44 square degrees, comprising VVV tiles b201 to b228. This area is sufficiently far from the Galactic plane that extinction and crowding do not present severe limitations.

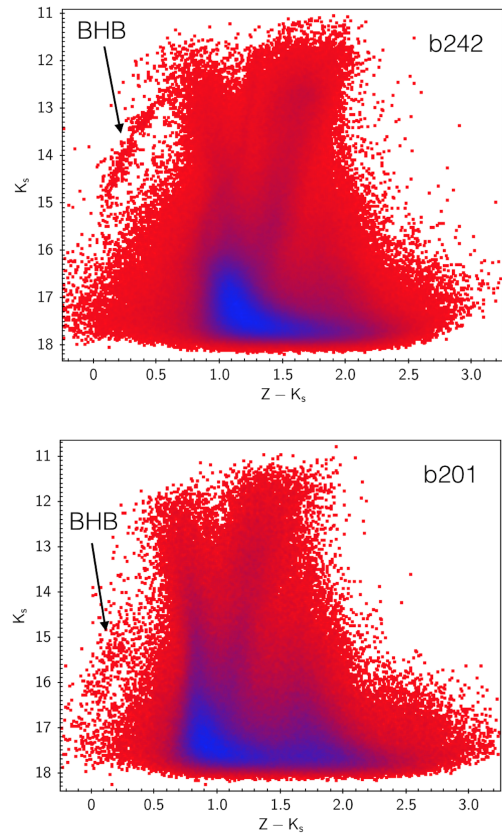


Figure 3. **Top panel:** CMD of the sources in tile b242, including the stars from globular cluster M22. BHB stars in M22 are clearly distinct at the bluest colors and brightest magnitudes. **Bottom panel:** CMD of the sources in tile b201, one of the fields included in our study. Bulge BHB stars are located at similar colors for M22, but about two magnitudes fainter.

2.2. Selection of BHB Stars

In order to select BHB stars in the bulge, one can fit theoretical isochrones to their CMDs (e.g., Brown et al. 2004). However, we preferred an empirical selection approach, since we needed to consider the presence of complex stellar populations as well. For that reason we use the globular cluster M22 (NGC 6656) as a standard sample, as it comprises an old stellar population with a prominent horizontal branch. This cluster was observed in the near-IR by the VVV in the same way, with the same instrumental setup, sharing the biases and constraints of our BHB star sample.

Given the known distance difference, the bulge BHB stars would be located in the CMD about two magnitudes fainter than the M22 BHB stars. The bulge BHB stars can be clearly seen in the deep VVV near-IR CMDs (Figure 3).

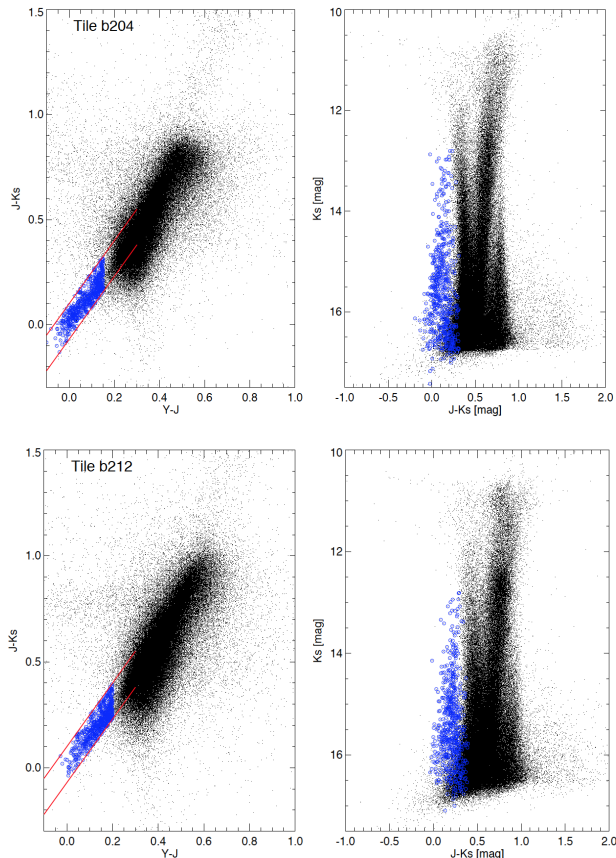


Figure 4. Top panels: Color-color and color-magnitude diagrams for the tile b204, with selected BHB stars marked in blue and color cuts of $Y - J < 0.15$ and $J - K_s < 0.35$. **Bottom panels:** Color-color and color-magnitude diagrams for the reddened tile b212, with selected BHB stars marked in blue and color cuts in $Y - J < 0.20$ and $J - K_s < 0.45$.

We used the $Y - J$ vs. $J - K_s$ color-color diagram to select bulge BHB stars, demanding $Y - J < 0.15$ and $J - K_s < 0.35$ (Figure 4). These cuts are applied in most fields, and only relaxed to $Y - J < 0.20$ and $J - K_s < 0.45$ in the most reddened fields, e.g. b212, which are contaminated by RGB stars from the Sgr dwarf galaxy.

At the faintest magnitudes there is contamination from other A-type stars (e.g. Brown et al. 2004 ; Clewley & Jarvis 2006). For example, some bulge blue straggler stars in particular share a similar location in the CMDs. Also, in these fields there is some contamination from the main sequence of the Sgr dSph galaxy. In order to take the contamination from A-type stars into account, we added another near-IR color cut: $J - H < 0.10$. This is because, according to Brown et al. (2004), the BHB stars have: $-0.20 < (J - H)_0 < 0.10$ and $-0.10 < (H - K)_0 < 0.10$ (Figure 5), with $J - H$ being a good indicator to discard A-type stars, since they

tend to have redder $(J - H)_0$ colors. Our final sample contains 12,554 bulge BHB star candidates.

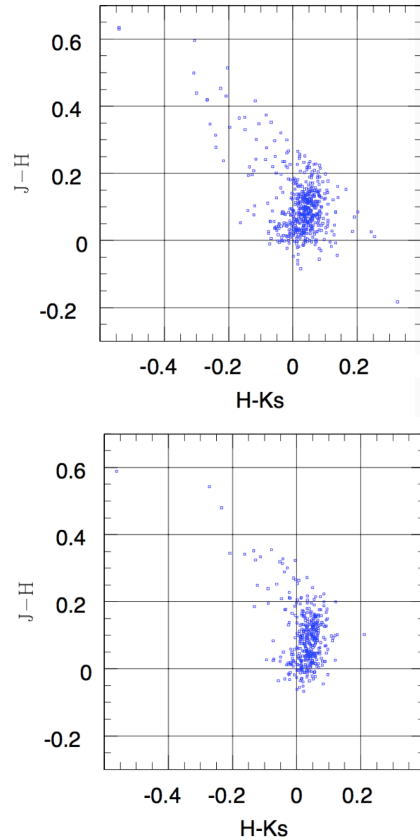


Figure 5. Color-color diagrams of selected BHB stars for tiles b207 (top panel) and b201 (bottom panel), according to the color cut suggested by Brown et al. (2004).

3. A SEARCH FOR NEW GLOBULAR CLUSTERS

Minniti et al. (2017 a,b,c) recently reported the discovery of dozens of new globular cluster candidates in the Galactic bulge. BHB stars are well known representative of old and metal-poor populations, often found in old globular clusters. Single Stellar Population (SSP) models tell us that, in a globular cluster, for every BHB star there are hundreds of red giant branch and thousands of main-sequence stars (even though recently it has been found that not all GCs are single stellar populations, see e.g. Piotto et al. 2005).

In this work we aim to detect over-densities of BHB stars in the selected 28 fields, since they may lead to the discovery of heretofore unknown globular clusters, and complement other stellar population studies. To accomplish this, we generated density maps of BHB candidates (Figure 6) with different bin sizes. We also generated random homogeneous samples of 12,554 points (equiv-

alent to the total number of BHB stars in our catalog), distributed across the 28 tiles. The results of these Monte Carlo simulations were plotted, together with the BHB stars of the sample. The objective was to analyze if there were over-densities that could correspond to previously undiscovered globular clusters or streams. We experimented with a number of different bin searches. Ultimately, from a density plot with hexagonal bins and a color gradient, we obtained a first-pass identification of possible over-densities. The size of each bin was chosen to be the average size that the typical globular clusters in our galaxy would have at the distance of the Galactic bulge.

According to [Chen & Chen \(2010\)](#), a typical Milky Way globular cluster has a size of $5 \text{ pc} \equiv 2'$ on the sky. Figure 6 (top panel) shows the panorama for the 28 tiles studied; some over-densities, mostly of low significance ($< 3\sigma$), are seen. Then we performed a new inspection, with a bin size of $12'$, which is a very large size for a globular cluster (1° could host 5 globular clusters). In Figure 6 (bottom panel) we can see some over-densities, but with a larger number of objects per bin than in the previous simulation. Also, we can see two probable streams close to the coordinates $\ell = 10^\circ$ and $\ell = 353^\circ$. Even though these over-densities are more significant, the result is unlikely to be successful in identifying any new clusters, since such a large globular cluster probably would have been discovered already. In addition, the streams we identify could be due to inhomogeneities in the reddening, as the BHB search is extremely sensitive to reddening variations. However, we point out that the stream at $\ell = 10^\circ$ could be associated with tidal tails from the globular cluster M22, located in tile b242, just outside this map, and which contains a rich population of BHB stars.

In order to study these over-densities more clearly, Monte Carlo simulations were performed for each tile, using as the sample the number of stars contained in each tile, plus the real stars in each of them. The most interesting results of each simulation are shown in Figures 7 and 8. This simple exercise shows that we have to report a negative result; even though there may be some over-densities, these are probably not due to previously unknown globular clusters. These over-densities could correspond to streams, which will be addressed in future work.

4. LIGHT CURVES

4.1. Variability

We search for variability by constructing light curves of all the BHB stars in our sample. In order to do this, additional data were needed, which were downloaded

from the VSA (VISTA Science Archive)¹ hosted on the Royal Observatory of Edinburgh website. Then, a cross-match was performed using the VSA and the original data available for each star. For each object there are on average 52 epochs; each magnitude has its respective error. Typical errors range from 0.01 to 0.06 mag at the brightest and faintest magnitudes of our sample, respectively.

The tiling pattern produces overlap regions between the tiles, corresponding to about 7% of the total VVV Survey area ([Saito et al. 2012b](#)). In these regions the data for each source are combined, thus producing light curves with double, or even four times more, data-points. In our sample 80 objects are in the overlap regions, with light curves reaching +100 epochs in total. In order to account for spuriously large photometric errors, we apply sigma clipping by eliminating the points are more than 3σ away from the mean of the light curve.

With this information, plots of amplitude versus magnitude were made (Figure 9 top panel), in order to find a suitable cut for the minimum amplitude that could yield a cleaner and easier to study light curve. A cut of minimum amplitude is set at $\text{Amp } K_s = 0.15 \text{ mag}$ for the light curves of interest, after a visual inspection of Figure 9 (top panel).

Finally, Figure 9 (bottom panel) shows the magnitudes of the selected BHB stars and their amplitudes, after cleaning the light curves, and applying the cut in amplitude. A total of 7,665 light curves were obtained using this criterion, which corresponds to 61% of the original sample and whose magnitudes are within the range $12.68 \leq K_s \leq 16.80$. The remaining 39% of the sample are BHB stars that do not exhibit variability, which are beyond the scope of this work, but these candidate stars are still being studied and will be presented in a future paper.

4.2. Period Searches

The Lomb-Scargle Periodogram ([Lomb 1976](#); [Scargle 1982](#)) is a statistical tool used to detect periodic signals in unevenly spaced observations; it works by making a search for the maximum peak in frequency of the light curve data. This estimating function was used to determine the period of our BHB stars' phased light curves.

An alias is a false period that contaminates the periodograms. In particular, daily aliases occur when the interval between observations matches the day/night cycle, half or some other multiple of this ([Scargle 1982](#); [Baluev 2012](#)). Observing the values obtained for the periods and the light curves of our sample of BHB stars,

¹ <http://horus.roe.ac.uk/vsa/>

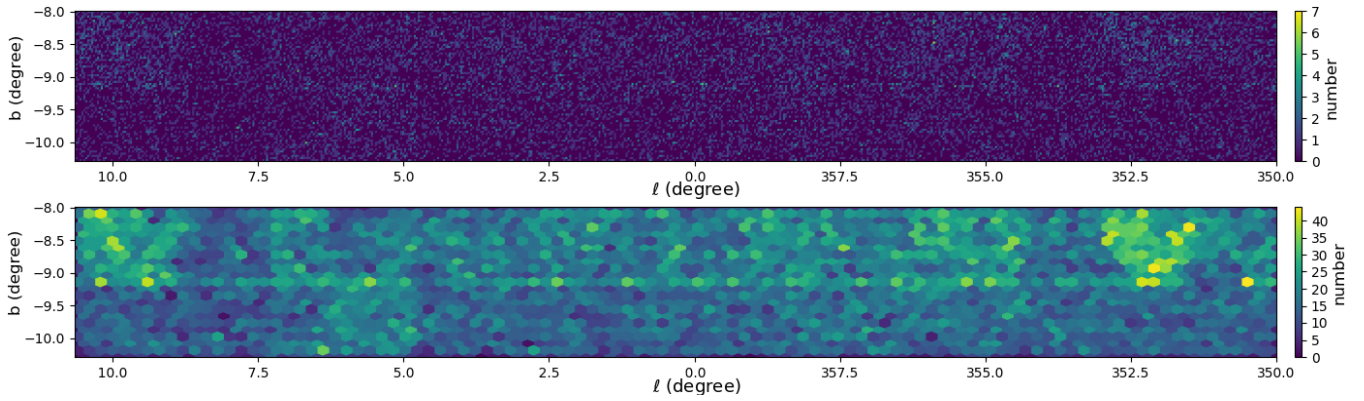


Figure 6. Top panel: Density plot for the 28 tiles, using a bin size = $2'$. In the clearest areas it is possible to note 97 over-densities, mostly of low significance. **Bottom panel:** An alternative density plot, with a bin size = $12'$. In the yellow areas it is possible to note 59 over-densities with a greater number of objects per bin, and two possible streams. Targets located in the overlap regions between tiles are accounted for twice in this plot, thus producing the artificial, horizontal over-density stripe seen crossing the plot at $b \sim 9.1^\circ$.

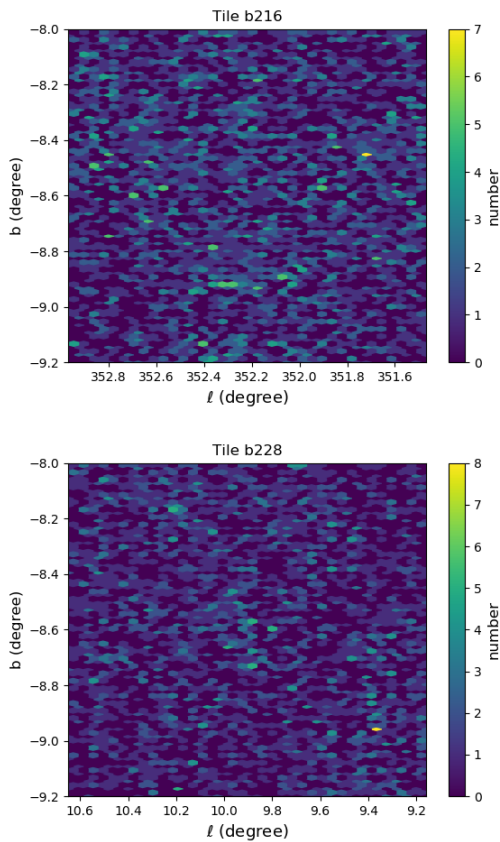


Figure 7. Some interesting over-densities corresponding to the first simulation (bin size of $2'$).

we find that 1,721 of them correspond to daily aliased periods between 0.1 and $3.\bar{3}$ days, being the most common alias of one day. These light curves, like the one shown in Figure 10, are left out of our analysis.

With a total of 5,944 good-quality light curves, we carried out a visual inspection at least three times, to

determine what kind of variable stars they were. Following the models exhibited by Prša et al. (2011), we detected a total of 336 eclipsing binaries (Figure 11). We classified 232 of them as first category (Figure 11 top panel), due to their error bars are on average 0.02 mag and the other 104 sources were classified as second category, because they exhibited error bars with an average of 0.04 mag (Figure 11 bottom panel). Regardless, all of them exhibit light curves that are sufficiently clear to distinguish them from other variable stars. The remaining 5,608 variable stars remain unclassified, until more epochs become available in their light curves.

We also found 12 RR Lyrae stars, such as that shown in Figure 12; all are listed in Table 3. Seven of these RR Lyrae were independently discovered by Gran et al. (2016), using a different selection method that does not consider the color of the stars as in this work. The remaining 5 RR Lyrae have bluer colors ($J - K_s \sim 0.27$). Considering the Hess diagram presented by Gran et al. (2016), our 5 RR Lyrae have colors within the color range of their stars.

4.3. Classification of Eclipsing Binaries

An eclipsing variable is a binary system with its orbital plane oriented edge-on towards the Earth, in such a way that eclipses and transits can occur. According to the General Catalogue of Variable Stars² (Samus et al. 2017), eclipsing binaries can be classified into three groups, depending on the shape of their light curves: EA (Algols), EB (β Lyrae), and EW (W Ursae Majoris).

From visual inspection, we classified a total of 42 EA eclipsing binaries, since these are different from the other two types, mainly due to the flat portion of their light

² <http://www.sai.msu.su/gcvs/gcvs/>

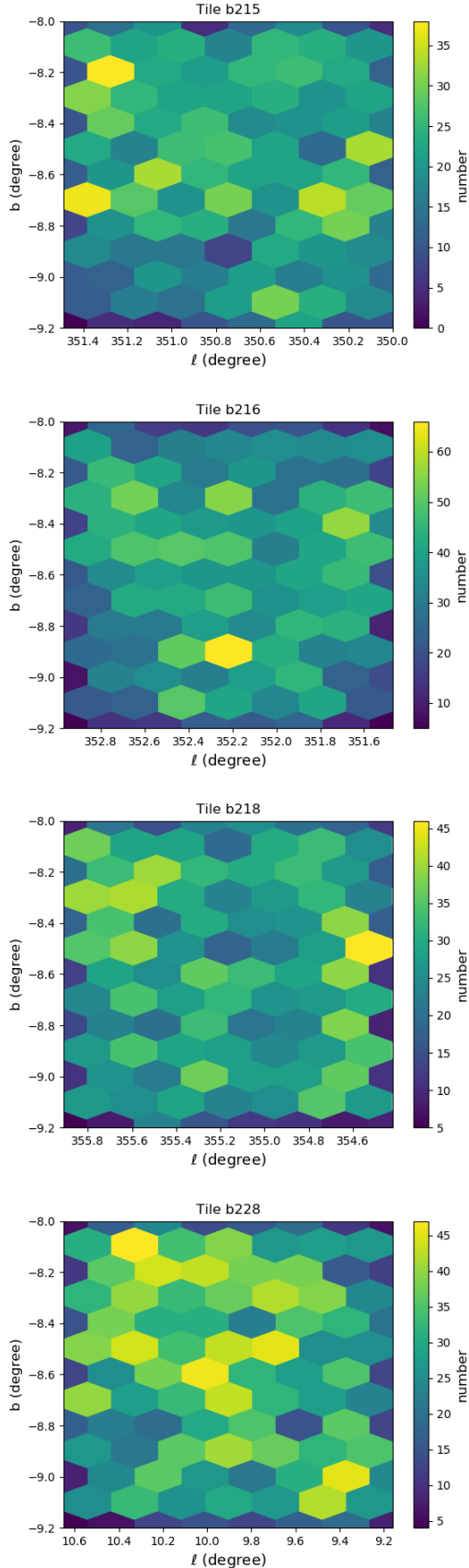


Figure 8. Some interesting over-densities corresponding to the second binning exercise (bin size of $12'$).

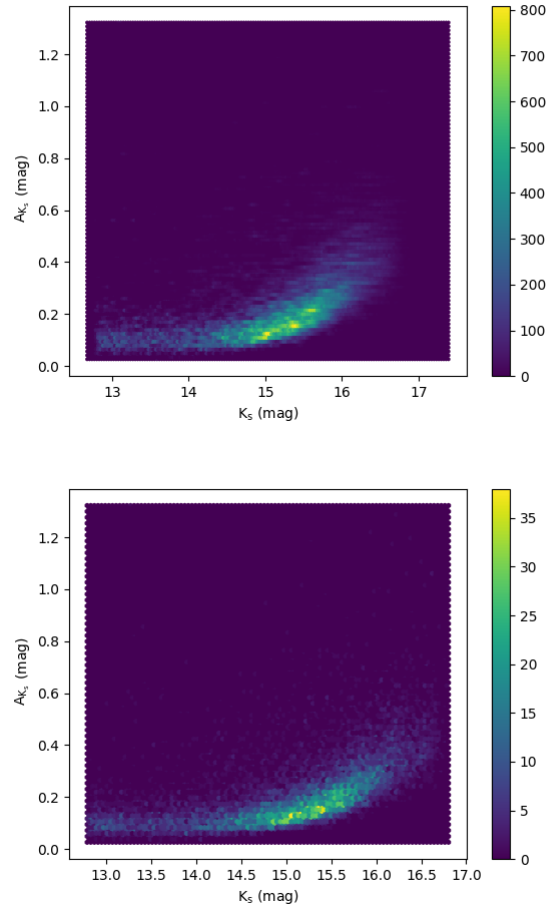


Figure 9. **Top panel:** Amplitude vs. K_s magnitude for the total sample of BHB stars. This plot allows us to determine a cut of minimum amplitude. **Bottom panel:** Amplitude of the light curve vs mean K_s magnitude after cleaning the light curve with our sigma clipping constraint, and applying the cut at $Amp K_s = 0.15$ mag.

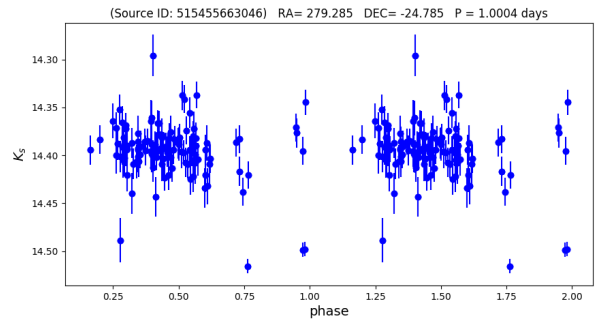


Figure 10. Example of a BHB star light curve with a daily aliased period.

curves. Then, to distinguish between the other two types, EB and EW, a deeper analysis is made, consid-

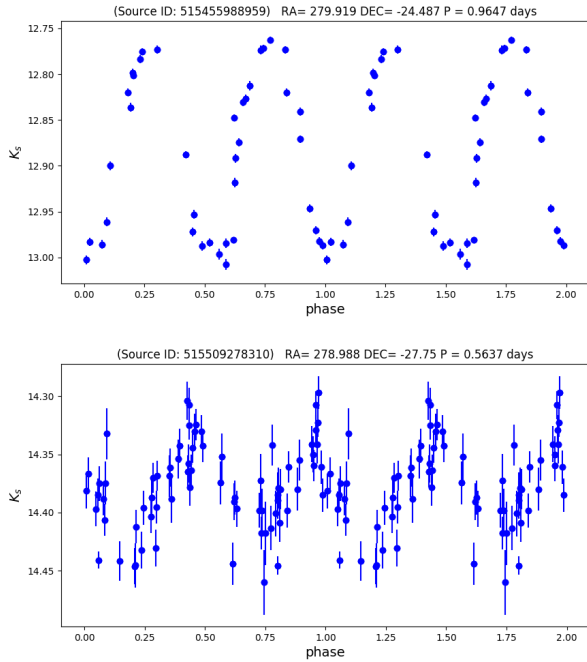


Figure 11. Top panel: light curve of a BHB star classified as a 1st category eclipsing binary. **Bottom panel:** light curve of a BHB star classified as a 2nd category eclipsing binary.

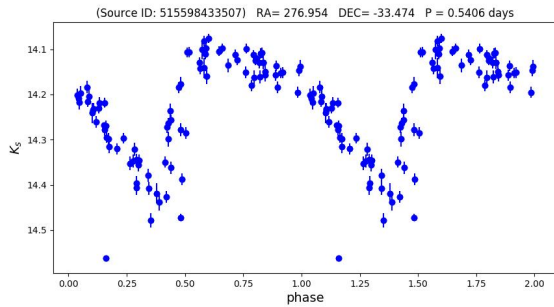


Figure 12. RR Lyrae star found in our sample.

ering their periods and amplitudes in addition to visual inspection of the light curve shape, thus obtaining 119 EB type and 175 EW type eclipsing binaries in our sample of BHB candidates in the outer bulge. Tables 1 and 2 present the characteristics (coordinates, periods, amplitudes, and magnitudes) of each of these candidate BHB eclipsing binary stars. Likewise, Figures 18 - 27 and 28 - 32 show the light curves of 1st and 2nd category examples of these 336 stars, respectively.

The region of the CMD occupied by the BHB stars is rich in variable stars, including eclipsing binaries, as recently shown by the Gaia satellite (Eyer et al. 2018). In particular, shorter period eclipsing binaries predom-

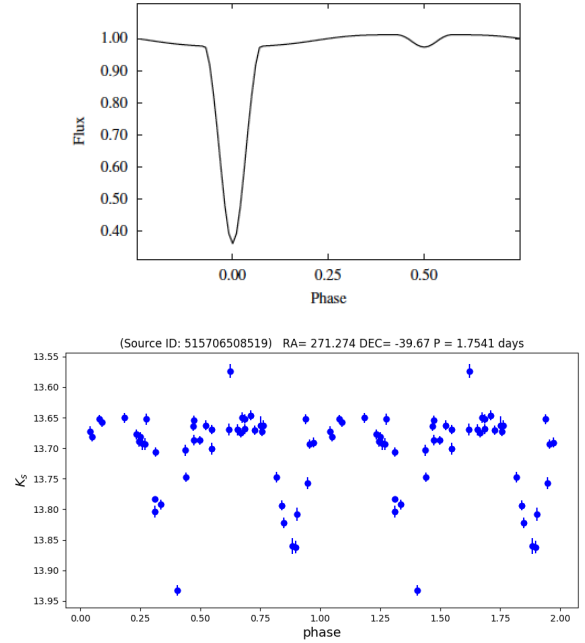


Figure 13. EA eclipsing binaries. A synthetic light curve (obtained from Kallrath & Milone 2009) in the top panel can be compared with one of our EA light curves shown in the bottom panel.

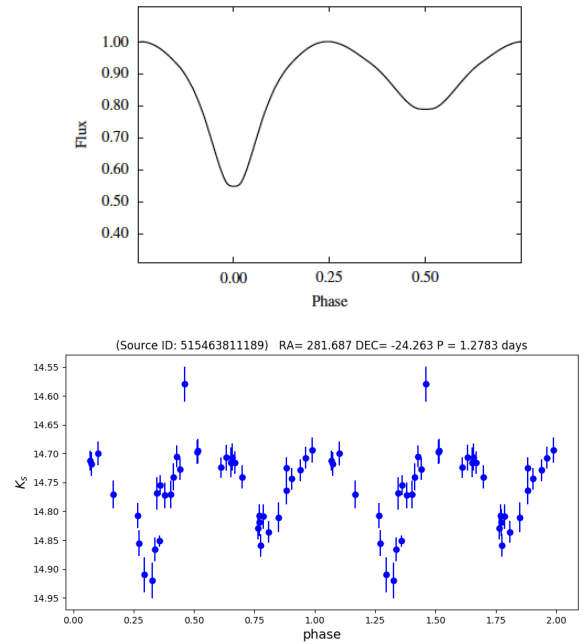


Figure 14. EB eclipsing binaries. A synthetic light curve (obtained from Kallrath & Milone 2009) in the top panel can be compared with one of our EB light curves in the bottom panel.

inate in our sample because they are easier to detect than longer period ones. As expected, the EWs are more

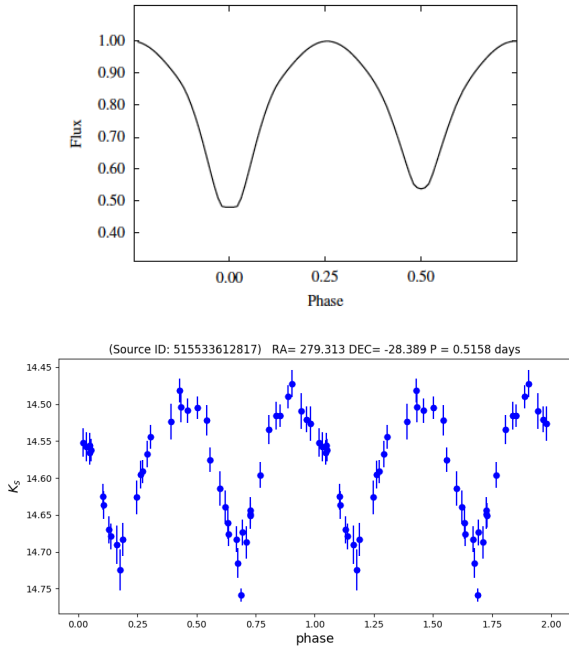


Figure 15. EW eclipsing binaries. A synthetic light curve (obtained from Kallrath & Milone 2009) in the top panel can be compared with one of our EW light curves in the lower panel.

concentrated towards shorter periods than the EAs and EBs.

4.4. Period-Amplitude Diagram

Bailey (1902) classified RR Lyrae stars by their periods and amplitudes of variation. Even now, the Period-Amplitude diagram (a.k.a. the Bailey diagram) is quite useful for the classification and study of the intrinsic properties of variable stars.

From inspection of the top panel of Figure 16, one can see that the periods of our eclipsing binaries span between $0.2 < P < 19.2$ days, and their amplitudes are in the range $0.15 < \text{Amp } K_s < 0.91$ mag. Eclipsing binaries, corresponding to 2.7% of the BHB stars original sample, are more homogeneously distributed than the remaining variable stars in the sample, which are strongly concentrated at low amplitudes and short periods. The average period is 1.12 days for eclipsing binaries, which is a similar value to that obtained by Rozycka et al. (2017) for 29 BHB stars that correspond to eclipsing binaries in the field of the globular cluster M22, which have an average period of 1.86 days.

According to the Gaia DR2 variable star color-magnitude diagram given by Eyer et al. (2018) (their Figure 4), there are eclipsing binaries present in the horizontal branch. For this reason, we decided to perform a cross-match between our sample of BHB eclipsing bi-

naries and the objects detected by Gaia DR2³ in this area of the Milky Way, considering only sources which were classified as variables. We found 100 matches in total, corresponding to about one third of our eclipsing binaries sample, which we consider a good confirmation of our results. We expect an increase in the number of matches when Gaia completes the classification of variable and non-variable objects in the area studied here.

From inspection of the bottom panel of Figure 16, one can see that the periods of the remaining variables are in the range $0.1 < P < 8.5$ days, and their amplitudes span between $0.15 < \text{Amp } K_s < 1.32$ mag. These variables stars, corresponding to 44.7% of the BHB candidates in the original sample, reach the highest amplitudes and periods, almost as long as the eclipsing binaries; an average period of 0.53 days. As expected, the 12 RR Lyrae found in our sample are included within the ranges of this part of the sample. In addition, in our sample, most of the long-period variables have smaller amplitudes, while short-period variables have larger amplitudes, on average.

In spite of their small numbers, our RR Lyrae are located in the Oosterhoff type I region of the Bailey diagram, different from the M22 RR Lyrae that are Oosterhoff type II. This is in agreement with the previous results of Gran et al. (2016), who analyzed the Bailey diagram for a thousand bulge RR Lyrae discovered by the VVV survey.

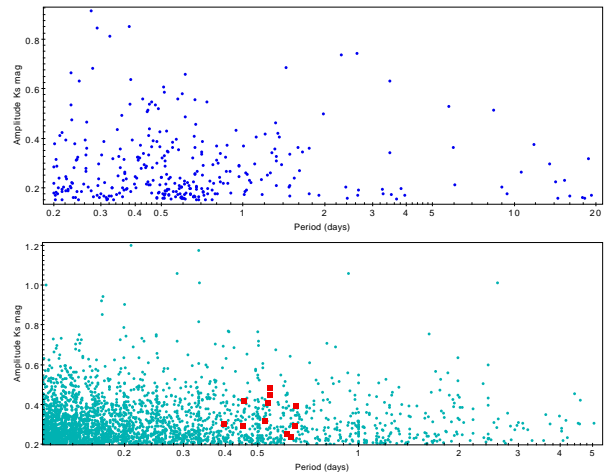


Figure 16. **Top panel:** Period-Amplitude diagram of eclipsing binaries from our sample. **Bottom panel:** Period-Amplitude diagram of the remaining variables. Turquoise points correspond to BHB stars and red squares are our 12 RR Lyrae.

³ <http://vizier.u-strasbg.fr/viz-bin/VizieR-3>

5. RESULTS

We have studied an area of 40 square degrees on the sky, in order to characterize the population of BHB stars in the direction of the Galactic bulge using VVV data. This area corresponds to 28 tiles of 1.1×1.5 square degrees each, in the bulge-halo transition region of the Milky Way. We discovered a total of 12,554 BHB candidate stars using a strict color selection, taking the BHB members of the old and metal-poor globular cluster M22 as a reference. The present bulge BHB catalog is used here to search for new globular clusters and variable stars.

Monte Carlo simulations were performed with the goal of detecting over-densities that could be undiscovered globular clusters, covering the total area first and then each tile individually. The first simulations used a bin size of $2'$ – some over-densities were discovered, but all of them were of low significance. The second simulation used an extreme bin size of $12'$ – some of the corresponding over-densities reveal two possible streams, whose analysis will be a part of future work.

We also examined the variability of the BHB sample, plotting light curves having an average of 52 epochs. By choosing as a minimum amplitude $\text{Amp } K_s = 0.15$ mag, we found 7,665 variable BHB candidates with mean magnitudes between $12.68 \leq K_s \leq 16.80$. Their mean magnitudes are consistent with the majority of them being located at the distance of the Galactic bulge, $d \approx 8$ kpc. Their periods were determined using the Lomb-Scargle periodogram, yielding an average of 1.12 days for eclipsing binaries and 0.53 days for the remaining variables. A total of 1,721 variable stars with aliased periods was detected, which were discarded. We performed a visual inspection of the remaining sample of 5,944 BHB stars, finding 336 good-quality eclipsing binary candidates, with periods up to $P = 19.2$ days. These were further sub-classified as detached, semi-contact, and con-

tact binaries (12.5 % EA, 35.4 % EB, 52.1 % EW). A total of 12 RR Lyrae were detected, including 7 of them that were independently discovered by [Gran et al. \(2016\)](#). From a period-amplitude diagram we found that the amplitude range for the remaining variables is $0.15 \leq \text{Amp } K_s \lesssim 1.32$ mag and $0.15 \leq \text{Amp } K_s \lesssim 0.91$ for eclipsing binaries, with a period range $0.1 < P < 8.5$ days for the remaining variables, and $0.2 < P < 19.2$ for eclipsing binaries.

Finally, comparing our sample of BHB stars with the study of RR Lyrae stars in the same region by [Gran et al. \(2016\)](#), we see that the Galactic bulge BHB population is more than an order of magnitude larger than that of the RR Lyrae ($\sim 14\times$).

The authors gratefully acknowledge the careful review of this manuscript by an anonymous referee, which contributed to clarification of our results. We also gratefully acknowledge the use of data from the ESO Public Survey program ID 179.B-2002 taken with the VISTA telescope, and data products from the Cambridge Astronomical Survey Unit (CASU). Support for the authors is provided by the BASAL Center for Astrophysics and Associated Technologies (CATA) through grant PFB-06, and the Ministry for the Economy, Development, and Tourism, Programa Iniciativa Científica Milenio through grant IC120009, awarded to the Millennium Institute of Astrophysics (MAS). D.M. acknowledges support from FONDECYT Regular grant No. 1170121. DM is also grateful for the hospitality of the Vatican Observatory. T.C.B. acknowledges partial support from grant PHY 14-30152 (Physics Frontier Center/JINAC-CEE), awarded by the U.S. National Science Foundation. T.C.B. is also grateful for funding from the Luksburg Foundation, which supported his travel to Chile in August, 2017, and enabled him to participate in this collaboration effort. J.A.-G. acknowledges support from FONDECYT Initiation grant 11150916.

REFERENCES

- Alonso-García, J., Dékány, I., Catelan, M., et al. 2015, *AJ*, 149, 99.
- Bailey, S.I. 1902, *Annals of Harvard College Observatory*, 38,1.
- Baluev, R. 2012, *MNRAS*, 422, 3.
- Beers, T.C., Preston, G.W., & Shectman, S.A. 1988, *ApJS*, 67, 461.
- Beers, T.C., Wilhelm, R.J., Doinidis, S.P., & Mattson, C. 1996, *ApJS*, 103, 433.
- Beers, T.C., Rossi, S., Wilhelm, R.J., et al. 2007, *ApJS*, 168, 277.
- Brown, W., Geller, M., Kenyon, S., et al. 2004, *ApJ*, 127, 1555.
- Brown, W., Beers, T.C., Wilhelm, R., et al. 2008, *AJ*, 135, 564.
- Busso, G., Moehler, S., Zoccali, M., Heber, U., & Yi, S. K. 2005, *ApJ*, 633, L29
- Carollo, D., Beers, T.C., Placco, V.M., et al. 2016, *Nat. Phys.*, 12, 1170
- Catelan, M., Minniti, D., Lucas, P. W., et al. 2011b, in *RR Lyrae Stars, Metal-Poor Stars, and the Galaxy*, ed. A. McWilliam, 145.

- Chen, C. W. & Chen, W. P. 2010, *ApJ*, 721, 1790.
- Christlieb, N., Beers, T.C., Thom, C., et al. 2005, *A&A*, 431, 143.
- Clewley, L., & Jarvis, M. J. 2006, *MNRAS*, 368(1), 310-320.
- Cross, N. J. G., Collins, R. S., Hambly, N. C., et al. 2009, *MNRAS*, 399, 1730.
- Cutri, R. M., Skrutskie, M. F., van Dyk, S., et al. 2003, *VizieR Online Data Catalog: II/246*
- Emerson, J., & Sutherland, W. 2010, *The Messenger*, 139, 2-5.
- Eyer, L., Rimoldini, L., Audard, M., et al. 2018, *A&A*, in press (arXiv:1804.09382).
- Gran, F., Minniti, D., Saito, R. K., et al. 2016, *A&A*, 591, A145.
- Hambly, N. C., Mann, R. G., Bond, I., et al. 2004, *Proc. SPIE*, 5493, 423.
- Hodgkin, S. T., Irwin, M. J., Hewett, P. C., & Warren, S. J. 2009, *MNRAS*, 394, 675.
- Irwin, M. J., Lewis, J., Hodgkin, S., 2004, *Proc. SPIE*, 5493, 411.
- Kallrath, J., & Milone, E. F., 2009, *Eclipsing binary stars: modeling and analysis* (p. 120). New York: Springer.
- Koch, A., McWilliam, A., Preston, G. W., & Thompson, I. B. 2016, *A&A*, 587, 124
- Lomb, N. R. 1976, *Ap&SS*, 39, 447.
- Minniti, D., Lucas, P. W., Emerson, J. P., et al. 2010, *New A*, 15, 433.
- Minniti, D., Palma, T., Dékány, I., et al 2017, *ApJL*, 838(1), L14.
- Minniti, D., Alonso-García, J., Braga, et al 2017, *RNAAS*, 1(1), 16.
- Minniti, D., Alonso-García, J., & Pullen, J. 2017, *RNAAS*, 1(1), 54.
- Peterson, R. C., Terndrup, D. M., Sadler, E. M., & Walker, A. R. 2001, *ApJ*, 547, 240
- Pier, J. R. 1982, *AJ*, 87, 1515-1526.
- Piotto, G., Villanova, S., Bedin, L. R., et al. 2005, *ApJ*, 621, 777.
- Preston, G.W., Sheckman, S.A., & Beers, T.C. 1991, *ApJ*, 375, 121.
- Prša, A., Batalha, N., Slawson, R. W., et al 2011, *AJ*, 141, 83.
- Rozyczka, M., Thompson, I. B., Pych, W., et al. 2017, arXiv preprint arXiv:1709.09572.
- Ruhland, C., Bell, E. F., Rix, H. W., & Xue, X. X. 2011, *ApJ*, 731(2), 119.
- Saito, R. K., Hempel, M., Minniti, D., et al. 2012, *A&A*, 537, A107.
- Saito, R. K., Minniti, D., Dias, B., et al. 2012, *A&A*, 544, A147.
- Samus N.N., Kazarovets E.V., Durlevich O.V., et al. *General Catalogue of Variable Stars: Version GCVS 5.1*, *Astron. Rep.*, 2017, 61(1), 80-88.
- Santucci, R.M., Beers, T.C., Placco, V.M., et al. 2015, *ApJL*, 813, L16
- Scargle, J. D. 1982, *ApJ*, 263, 835.
- Smith, K. W., Bailer-Jones, C. A., Klement, R. J., & Xue, X. X. 2010, *A&A*, 522, A88.
- L. C. Smith, P. W. Lucas, R. Kurtev, et al. 2018, *MNRAS*, 474, 1826, arXiv:1710.08919.
- Sommer-Larsen, J., Beers, T.C., Flynn, C., et al. 1997, *ApJ*, 481, 775.
- Terndrup, D. M., An, D., Hansen, A., et al. 2004, *Ap&SS*, 291, 247
- Thom, C., Flynn, C., Bessell, M., et al. 2005, *MNRAS*, 360, 354.
- Xue, X.-X., Rix H.-W., Zhao, G., et al. 2008, *ApJ*, 684, 1143.
- Yanny, B., et al. 2009, *AJ*, 137, 4377.
- York, D. G, et al. 2000, *AJ*, 120, 1579.
- Zoccali, M., Renzini, A., Ortolani, S., et al. 2003, *A&A*, 399, 931

APPENDIX

Table 1. Complete Parameters for the First Category Eclipsing Binaries

VVV ID	RA(J2000)	DEC(J2000)	Period	A_{K_s}	Z	Y	J	H	K_s	Class
VVV 515455705782	18:41:02.6	-25:08:27.6	3.2937	0.18	14.75	14.93	14.51	14.24	14.12	EB
VVV 515455735619	18:37:32.4	-24:42:03.6	14.4274	0.16	15.20	15.38	15.04	14.93	14.82	EB
VVV 515455749525	18:40:50.8	-25:02:27.6	1.0277	0.19	15.67	15.80	15.53	15.35	15.27	EB
VVV 515455859192	18:38:27.6	-24:35:16.8	0.7135	0.29	14.74	14.92	14.52	14.29	14.17	EB
VVV 515455988959	18:39:40.5	-24:29:13.2	0.9647	0.25	13.47	13.66	13.23	12.98	12.85	EW
VVV 515456105530	18:41:39.6	-24:29:24.0	1.0014	0.37	15.13	15.31	14.94	14.75	14.63	EA
VVV 515456121023	18:41:49.6	-24:28:48.0	0.7075	0.39	15.45	15.61	15.25	15.01	14.92	EB
VVV 515456130441	18:42:31.9	-24:32:24.0	0.6329	0.21	14.23	14.40	14.09	13.88	13.80	EB
VVV 515456133444	18:40:15.1	-24:17:02.4	0.5331	0.19	15.37	15.59	15.13	14.81	14.77	EW
VVV 515456170484	18:39:16.0	-24:06:28.8	0.3856	0.64	13.84	14.02	13.61	13.39	13.27	EB
VVV 515456321480	18:39:37.9	-23:51:57.6	0.3584	0.20	15.25	15.43	15.02	14.77	14.67	EW
VVV 515456400097	18:40:07.2	-23:45:50.4	0.2797	0.68	15.00	15.22	14.75	14.49	14.36	EA
VVV 515456415489	18:39:54.7	-23:42:32.4	0.6560	0.17	15.09	15.26	14.91	14.65	14.60	EW
VVV 515456415913	18:40:14.4	-23:44:42.0	1.3856	0.29	15.46	15.64	15.23	15.04	14.95	EB
VVV 515456449481	18:43:15.8	-24:00:32.4	0.6228	0.22	13.81	14.00	13.59	13.32	13.22	EB
VVV 515456468492	18:42:26.4	-23:52:51.6	0.6544	0.16	15.82	16.00	15.61	15.41	15.35	EB
VVV 515456477398	18:40:56.8	-23:41:56.4	0.8028	0.18	14.08	14.24	13.87	13.64	13.53	EW
VVV 515463238313	18:46:23.0	-25:23:31.2	0.2992	0.18	14.38	14.52	14.24	14.07	14.00	EB
VVV 515463254012	18:43:26.4	-25:02:42.0	0.4402	0.22	15.28	15.45	15.14	15.03	14.94	EW
VVV 515463397605	18:46:41.5	-25:06:43.2	0.2809	0.17	13.27	13.41	13.08	12.89	12.81	EA
VVV 515463408991	18:44:39.8	-24:52:15.6	0.6844	0.15	14.46	14.62	14.26	14.02	13.93	EW
VVV 515463439496	18:43:10.5	-24:38:52.8	0.7726	0.29	15.85	16.00	15.70	15.62	15.48	EB
VVV 515463474152	18:45:03.5	-24:46:51.6	0.3703	0.19	14.18	14.33	13.99	13.71	13.62	EW
VVV 515463627153	18:47:35.0	-24:44:24.0	14.2106	0.22	15.86	16.01	15.66	15.40	15.39	EW
VVV 515463638100	18:46:14.8	-24:34:33.6	0.4088	0.32	15.04	15.20	14.89	14.67	14.61	EB
VVV 515463811189	18:46:44.8	-24:15:46.8	1.2783	0.34	15.28	15.47	15.10	14.85	14.76	EB
VVV 515479196684	18:38:20.3	-25:12:21.6	0.2050	0.31	15.75	15.93	15.73	15.64	15.62	EB
VVV 515485761639	18:41:21.5	-26:45:43.2	0.5158	0.19	14.44	14.59	14.30	14.11	14.02	EB
VVV 515485890589	18:43:36.7	-26:45:10.8	0.9443	0.43	16.35	16.45	16.28	16.19	16.22	EW
VVV 515486229451	18:43:38.8	-26:05:13.2	0.6410	0.18	15.00	15.20	14.81	14.54	14.43	EW
VVV 515502700536	18:34:23.5	-27:42:46.8	0.2948	0.16	14.41	14.58	14.25	14.08	13.97	EW
VVV 515502774251	18:31:57.6	-27:16:22.8	0.4820	0.16	15.55	15.70	15.39	15.23	15.20	EB
VVV 515502854285	18:34:11.2	-27:19:19.2	0.7078	0.25	15.67	15.81	15.61	15.55	15.50	EB
VVV 515502982294	18:35:32.1	-27:09:32.4	1.0221	0.26	14.76	14.94	14.59	14.37	14.28	EW
VVV 515503005741	18:35:07.6	-27:03:28.8	0.5140	0.17	15.37	15.52	15.25	15.19	15.09	EA
VVV 515503015717	18:34:20.8	-26:56:52.8	1.4859	0.21	15.31	15.47	15.11	14.89	14.85	EB
VVV 515503031413	18:36:47.2	-27:10:22.8	1.3593	0.40	14.29	14.44	14.11	13.90	13.82	EW
VVV 515503064540	18:35:39.6	-26:58:19.2	0.8436	0.22	15.42	15.56	15.25	15.06	14.96	EW
VVV 515503126545	18:34:37.1	-26:42:32.4	0.6082	0.21	13.91	14.05	13.72	13.52	13.43	EB
VVV 515503155742	18:36:21.5	-26:49:22.8	0.2532	0.19	14.95	15.16	14.77	14.62	14.53	EB
VVV 515509335060	18:37:59.7	-27:52:22.8	0.5265	0.19	15.13	15.31	14.97	14.81	14.77	EB
VVV 515509419626	18:40:02.8	-27:56:38.4	0.2316	0.66	16.02	16.13	15.87	15.69	15.69	EA
VVV 515509629158	18:37:32.6	-27:19:01.2	10.6049	0.26	16.06	16.21	15.89	15.70	15.67	EW
VVV 515509680856	18:41:40.5	-27:39:43.2	3.4843	0.63	15.52	15.66	15.37	15.19	15.06	EA
VVV 515509805739	18:42:06.7	-27:29:13.2	0.4183	0.37	15.90	16.01	15.79	15.61	15.55	EW
VVV 515509902878	18:38:19.4	-26:54:28.8	0.5405	0.24	15.06	15.26	14.86	14.60	14.49	EW
VVV 515510032922	18:40:40.8	-26:54:36.0	0.6137	0.15	15.67	15.86	15.53	15.37	15.25	EW
VVV 515524680472	18:29:35.5	-28:34:51.6	0.9881	0.25	14.33	14.50	14.15	13.96	13.88	EB
VVV 515524928629	18:30:25.2	-28:13:26.4	0.7385	0.18	14.17	14.28	14.09	14.03	13.99	EB
VVV 515532803859	18:34:46.8	-29:17:06.0	5.9534	0.36	16.17	16.43	16.03	15.76	15.83	EB

Table 1 continued

Table 1 (continued)

VVV ID	RA(J2000)	DEC(J2000)	Period	A_{K_s}	Z	Y	J	H	K_s	Class
VVV 515532862233	18:36:48.2	-29:24:43.2	1.0337	0.25	15.50	15.62	15.35	15.11	15.03	EB
VVV 515532888963	18:36:43.6	-29:21:57.6	0.5500	0.38	16.10	16.22	16.05	15.83	15.89	EW
VVV 515532894334	18:37:28.0	-29:26:06.0	0.5925	0.20	15.41	15.54	15.23	15.04	14.97	EW
VVV 515532900637	18:35:16.8	-29:11:49.2	0.2236	0.24	15.28	15.41	15.13	14.93	14.87	EW
VVV 515533142460	18:37:48.7	-29:07:04.8	0.4220	0.28	16.19	16.32	16.08	15.89	15.89	EW
VVV 515533399455	18:37:33.6	-28:43:30.0	0.8998	0.18	15.41	15.58	15.25	15.04	14.95	EW
VVV 515533483785	18:35:24.4	-28:22:37.2	0.5525	0.18	14.87	14.99	14.76	14.65	14.59	EB
VVV 515533516155	18:36:42.7	-28:28:12.0	0.6392	0.17	15.17	15.31	15.03	14.87	14.79	EW
VVV 515533612817	18:37:15.1	-28:23:20.4	0.5158	0.29	15.15	15.30	14.98	14.76	14.67	EW
VVV 515533623705	18:35:01.6	-28:08:13.2	0.5229	0.43	15.44	15.58	15.26	15.06	15.02	EW
VVV 515533685022	18:36:08.4	-28:09:46.8	0.5934	0.16	15.05	15.21	14.87	14.65	14.55	EW
VVV 515533691114	18:37:21.3	-28:16:55.2	1.1678	0.23	13.38	13.53	13.20	13.01	12.91	EA
VVV 515533720615	18:36:41.0	-28:09:57.6	1.2645	0.26	15.77	15.86	15.72	15.68	15.63	EW
VVV 515533819516	18:39:57.8	-28:21:43.2	3.8242	0.20	15.64	15.78	15.58	15.45	15.40	EW
VVV 515533854339	18:39:53.5	-28:18:07.2	0.2157	0.19	15.11	15.33	14.95	14.69	14.62	EB
VVV 515537426340	18:26:42.2	-29:15:03.6	0.5921	0.20	15.04	15.19	14.89	14.73	14.63	EB
VVV 515546725524	18:29:31.4	-30:23:52.8	0.5849	0.24	15.59	15.72	15.40	15.17	15.14	EB
VVV 515546847685	18:27:29.0	-29:58:08.4	0.8199	0.24	15.20	15.36	15.08	14.92	14.85	EW
VVV 515546865778	18:29:50.4	-30:11:24.0	1.0683	0.22	15.26	15.38	15.10	14.91	14.83	EB
VVV 515547042083	18:27:16.3	-29:36:50.4	0.7049	0.34	14.26	14.38	14.09	13.89	13.83	EW
VVV 515547090761	18:27:18.2	-29:32:02.3	1.5487	0.24	15.46	15.59	15.36	15.22	15.15	EW
VVV 515547128073	18:28:42.0	-29:37:04.8	1.3303	0.31	15.18	15.37	14.98	14.70	14.63	EB
VVV 515547201799	18:28:02.8	-29:25:30.0	0.6595	0.17	14.35	14.50	14.16	13.93	13.85	EW
VVV 515547264576	18:28:47.7	-29:23:52.8	0.4521	0.54	16.50	16.68	16.44	16.25	16.29	EW
VVV 515547335356	18:27:32.1	-29:08:16.8	6.0382	0.21	15.97	16.13	15.80	15.65	15.57	EB
VVV 515547550143	18:30:15.3	-29:02:42.0	0.7180	0.17	14.54	14.69	14.35	14.14	14.05	EB
VVV 515556253152	18:33:37.6	-30:47:24.0	0.4757	0.53	15.47	15.58	15.35	15.15	15.09	EB
VVV 515556254998	18:33:50.1	-30:48:32.4	0.5884	0.16	14.70	14.81	14.55	14.40	14.37	EW
VVV 515556287416	18:32:49.6	-30:38:49.2	0.4923	0.42	14.39	14.52	14.25	14.06	13.97	EA
VVV 515556597046	18:33:37.2	-30:09:07.2	18.1572	0.16	15.73	15.84	15.62	15.52	15.46	EW
VVV 515556780207	18:35:13.4	-29:58:51.6	0.7887	0.18	14.48	14.64	14.34	14.10	14.03	EB
VVV 515556786026	18:32:32.1	-29:41:16.8	0.5123	0.59	15.69	15.81	15.58	15.44	15.36	EB
VVV 515556868176	18:33:52.3	-29:39:43.2	15.2890	0.23	15.94	16.09	15.81	15.72	15.64	EW
VVV 515557032064	18:33:05.0	-29:16:30.0	8.9788	0.20	15.55	15.71	15.41	15.33	15.25	EW
VVV 515560749810	18:23:10.0	-30:47:27.6	1.2303	0.25	14.99	15.16	14.82	14.58	14.50	EB
VVV 515568341628	18:22:54.2	-31:20:06.0	0.5106	0.61	14.94	15.06	14.81	14.62	14.54	EA
VVV 515568557768	18:27:37.4	-31:29:13.2	0.7707	0.19	14.32	14.43	14.16	14.02	13.96	EA
VVV 515568709317	18:27:29.5	-31:14:06.0	0.6722	0.20	14.76	14.87	14.60	14.41	14.31	EB
VVV 515568758126	18:23:59.2	-30:46:51.6	9.3822	0.18	15.27	15.40	15.11	14.94	14.86	EW
VVV 515569107954	18:24:50.6	-30:18:32.4	0.6648	0.26	15.37	15.56	15.19	14.99	14.88	EW
VVV 515569188676	18:25:24.4	-30:13:22.8	0.2929	0.30	15.12	15.30	15.02	14.98	14.89	EA
VVV 515569289548	18:27:27.3	-30:16:33.6	1.4878	0.17	14.35	14.53	14.18	13.97	13.87	EB
VVV 515577492549	18:27:17.7	-31:37:26.4	0.5339	0.24	13.51	13.60	13.38	13.19	13.14	EB
VVV 515577557342	18:30:43.2	-31:49:48.0	1.5925	0.36	16.34	16.38	16.30	16.27	16.27	EW
VVV 515577618447	18:31:14.6	-31:44:27.6	0.7542	0.23	15.27	15.41	15.16	15.00	14.92	EB
VVV 515577630181	18:28:24.2	-31:25:08.4	0.4808	0.39	16.72	16.97	16.70	16.56	16.65	EW
VVV 515577684111	18:30:17.5	-31:29:42.0	0.8656	0.27	15.58	15.67	15.55	15.51	15.45	EW
VVV 515577822273	18:31:50.4	-31:19:44.4	0.4384	0.28	15.98	16.03	15.95	15.93	15.95	EW
VVV 515578028901	18:31:02.4	-30:46:01.2	0.5983	0.16	15.14	15.31	15.01	14.79	14.71	EW
VVV 515578046934	18:30:21.6	-30:39:21.6	0.3636	0.19	14.50	14.61	14.51	14.47	14.44	EW
VVV 515578062813	18:33:10.8	-30:54:28.8	0.7679	0.15	14.91	15.06	14.78	14.60	14.54	EW
VVV 515589460543	18:23:11.5	-33:01:15.6	0.7974	0.37	15.81	15.98	15.68	15.48	15.44	EW
VVV 515589565303	18:21:26.8	-32:35:38.4	0.5141	0.17	15.64	15.79	15.45	15.21	15.17	EW
VVV 515589763733	18:21:57.1	-32:12:07.2	0.5075	0.17	13.26	13.36	13.10	12.91	12.84	EW

Table 1 continued

Table 1 (continued)

VVV ID	RA(J2000)	DEC(J2000)	Period	A_{K_s}	Z	Y	J	H	K_s	Class
VVV 515589955361	18:24:46.3	-32:04:08.4	0.7365	0.55	16.01	16.15	15.90	15.81	15.69	EW
VVV 515590034822	18:24:49.6	-31:53:06.0	1.6133	0.27	13.69	13.86	13.64	13.53	13.50	EB
VVV 515598605262	18:29:20.4	-33:12:25.2	0.3262	0.17	15.11	15.23	14.99	14.85	14.81	EW
VVV 515598683018	18:27:30.4	-32:49:58.8	0.4541	0.21	14.00	14.11	13.86	13.63	13.56	EW
VVV 515598788186	18:29:12.7	-32:44:52.8	0.7107	0.18	15.61	15.75	15.50	15.31	15.24	EB
VVV 515598789635	18:28:00.2	-32:37:15.6	0.2441	1.01	16.76	17.11	16.74	16.53	16.63	EW
VVV 515598953339	18:30:58.0	-32:31:22.8	0.3483	0.33	15.88	15.96	15.86	15.83	15.85	EB
VVV 515612100798	18:17:32.1	-33:57:18.0	2.6460	0.17	15.34	15.47	15.19	14.97	14.89	EW
VVV 515612225118	18:17:24.9	-33:44:31.2	0.5804	0.21	16.00	16.12	15.82	15.64	15.59	EB
VVV 515612284529	18:19:57.1	-33:55:12.0	0.5778	0.35	13.79	13.92	13.64	13.45	13.37	EB
VVV 515612392825	18:21:43.9	-33:55:51.6	1.3269	0.32	14.63	14.76	14.51	14.32	14.26	EW
VVV 515612471994	18:22:03.8	-33:50:38.4	0.9684	0.29	14.51	14.63	14.34	14.15	14.08	EW
VVV 515612652483	18:18:59.7	-33:14:09.6	1.0105	0.17	14.99	15.16	14.83	14.63	14.51	EW
VVV 515612816207	18:22:23.7	-33:20:31.2	1.3269	0.21	14.94	15.05	14.76	14.57	14.49	EB
VVV 515612881677	18:20:24.4	-33:01:48.0	0.5017	0.32	13.66	13.79	13.48	13.30	13.22	EA
VVV 515613006615	18:19:54.9	-32:46:48.0	0.5495	0.36	14.60	14.74	14.43	14.19	14.11	EB
VVV 515619875935	18:20:53.7	-34:21:50.4	0.7042	0.33	15.91	16.02	15.80	15.66	15.63	EW
VVV 515619876417	18:24:34.3	-34:44:20.4	0.6858	0.16	15.37	15.45	15.31	15.17	15.14	EW
VVV 515619884872	18:25:41.2	-34:50:02.4	0.4105	0.32	15.36	15.40	15.34	15.34	15.33	EB
VVV 515619887059	18:20:36.9	-34:18:50.4	0.4149	0.32	15.68	15.79	15.50	15.26	15.26	EW
VVV 515619955260	18:25:00.4	-34:38:06.0	0.4930	0.21	14.43	14.54	14.29	14.07	14.00	EB
VVV 515620070467	18:25:10.3	-34:26:06.0	0.5430	0.16	15.34	15.46	15.20	14.97	14.91	EB
VVV 515620091749	18:21:56.1	-34:03:57.6	0.5687	0.18	15.38	15.51	15.23	15.00	14.95	EB
VVV 515620145628	18:22:42.0	-34:02:45.6	0.4986	0.24	15.30	15.41	15.16	14.97	14.90	EB
VVV 515620146750	18:24:56.8	-34:16:19.2	0.5233	0.19	15.95	16.09	15.81	15.62	15.56	EB
VVV 515620257313	18:23:37.4	-33:56:09.6	0.4596	0.55	14.92	15.07	14.80	14.60	14.54	EB
VVV 515620469165	18:23:00.2	-33:28:55.2	0.6566	0.22	15.24	15.36	15.13	14.97	14.90	EW
VVV 515620492480	18:23:04.8	-33:26:49.2	0.3519	0.36	15.25	15.36	15.07	14.86	14.79	EW
VVV 515628733586	18:13:08.8	-34:52:44.4	0.4588	0.37	14.64	14.80	14.49	14.30	14.23	EB
VVV 515628750366	18:13:09.1	-34:51:07.2	0.5305	0.34	15.22	15.28	15.06	14.88	14.80	EB
VVV 515634464796	18:17:17.5	-35:38:02.4	0.8930	0.27	15.77	15.90	15.60	15.34	15.32	EW
VVV 515634544364	18:17:34.0	-35:31:08.4	1.2047	0.42	14.40	14.48	14.27	14.09	14.03	EW
VVV 515634710418	18:15:28.5	-35:01:58.8	0.2632	0.33	14.37	14.48	14.32	14.20	14.20	EB
VVV 515634747073	18:14:45.3	-34:53:02.4	0.5133	0.16	14.98	15.13	14.80	14.61	14.55	EW
VVV 515634816754	18:18:27.1	-35:09:14.4	0.4438	0.51	14.94	15.07	14.80	14.64	14.56	EB
VVV 515635036607	18:14:57.3	-34:24:54.0	0.4812	0.16	13.33	13.43	13.15	12.94	12.89	EA
VVV 515635039975	18:15:04.8	-34:25:15.6	0.8806	0.22	16.10	16.22	15.98	15.80	15.79	EW
VVV 515635293657	18:16:35.0	-34:08:34.8	0.6391	0.20	15.15	15.28	14.98	14.84	14.77	EW
VVV 515635386214	18:20:15.6	-34:22:40.8	0.6119	0.49	15.96	16.22	15.92	15.82	15.80	EW
VVV 515635391205	18:18:54.2	-34:13:48.0	0.7112	0.18	14.40	14.54	14.23	14.01	13.95	EB
VVV 515640862943	18:20:41.7	-35:50:27.6	1.9673	0.50	15.94	16.06	15.86	15.75	15.73	EW
VVV 515640980485	18:21:34.3	-35:42:10.8	0.5850	0.18	15.43	15.55	15.29	15.11	15.07	EB
VVV 515641169164	18:22:12.9	-35:24:21.6	1.4437	0.68	16.35	16.48	16.29	16.21	16.23	EW
VVV 515641257529	18:21:46.5	-35:11:34.8	0.4588	0.18	14.28	14.42	14.14	13.97	13.89	EW
VVV 515641270386	18:21:21.1	-35:07:33.6	0.6054	0.16	15.21	15.33	15.08	14.92	14.89	EB
VVV 515641398175	18:23:37.4	-35:06:18.0	0.2154	0.15	14.10	14.22	14.00	13.81	13.76	EW
VVV 515641453963	18:21:10.3	-34:45:03.6	0.6652	0.36	15.59	15.71	15.51	15.33	15.34	EW
VVV 515641567374	18:21:32.1	-34:34:01.2	0.5263	0.35	15.15	15.30	15.02	14.83	14.79	EB
VVV 515641571472	18:23:19.2	-34:44:20.4	0.4873	0.52	15.62	15.78	15.51	15.37	15.29	EB
VVV 515641577000	18:21:47.5	-34:34:30.0	1.1202	0.41	14.64	14.73	14.49	14.26	14.18	EA
VVV 515655720692	18:12:30.0	-36:27:54.0	0.6377	0.20	15.21	15.35	15.04	14.81	14.76	EA
VVV 515655774433	18:12:10.0	-36:20:45.6	0.6747	0.15	14.91	15.02	14.75	14.54	14.50	EB
VVV 515655788219	18:11:06.9	-36:12:50.4	0.6729	0.21	15.32	15.42	15.17	14.99	14.93	EB
VVV 515655853662	18:12:19.9	-36:14:20.4	0.5124	0.33	15.54	15.59	15.49	15.48	15.42	EA

Table 1 continued

Table 1 (continued)

VVV ID	RA(J2000)	DEC(J2000)	Period	A_{K_s}	Z	Y	J	H	K_s	Class
VVV 515656169262	18:16:00.0	-36:07:22.8	0.4309	0.29	15.62	15.75	15.49	15.26	15.25	EB
VVV 515656280990	18:13:46.8	-35:42:43.2	0.4489	0.33	15.96	16.10	15.89	15.83	15.80	EW
VVV 515656451877	18:15:26.1	-35:36:25.2	1.3087	0.36	13.72	13.85	13.56	13.34	13.28	EA
VVV 515660323166	18:17:33.6	-37:12:57.6	0.6794	0.27	14.55	14.67	14.42	14.25	14.20	EA
VVV 515660415049	18:17:15.8	-37:00:10.8	0.4461	0.51	16.35	16.36	16.37	16.36	16.45	EA
VVV 515660451890	18:15:48.7	-36:47:06.0	3.9586	0.17	15.60	15.67	15.60	15.59	15.61	EW
VVV 515660479408	18:17:11.2	-36:52:15.6	1.4811	0.20	14.62	14.73	14.49	14.36	14.32	EB
VVV 515660793090	18:18:15.3	-36:21:10.8	0.6648	0.56	15.88	16.00	15.77	15.59	15.54	EB
VVV 515660822975	18:18:51.1	-36:21:00.0	0.2627	0.27	16.31	16.38	16.17	16.04	15.99	EW
VVV 515660825897	18:17:47.2	-36:14:20.4	5.7477	0.53	14.19	14.32	14.08	13.90	13.84	EA
VVV 515672613993	18:06:13.9	-37:38:24.0	0.8711	0.37	15.62	15.74	15.46	15.27	15.18	EW
VVV 515672621619	18:06:34.5	-37:39:39.6	1.0527	0.23	15.45	15.57	15.28	15.06	14.98	EW
VVV 515672633444	18:07:01.4	-37:41:06.0	1.1003	0.30	14.10	14.24	13.94	13.70	13.65	EA
VVV 515672897820	18:08:06.7	-37:17:13.2	0.5949	0.16	15.10	15.24	14.95	14.78	14.72	EW
VVV 515672945875	18:12:18.9	-37:37:40.8	0.5052	0.16	14.83	14.95	14.65	14.45	14.41	EW
VVV 515672970884	18:07:33.3	-37:05:06.0	0.8248	0.22	15.31	15.44	15.18	15.01	14.95	EB
VVV 515672972715	18:08:06.4	-37:08:24.0	0.4402	0.29	15.96	16.02	15.90	15.83	15.81	EW
VVV 515672992986	18:08:48.7	-37:10:37.2	0.4298	0.34	14.97	15.09	14.80	14.61	14.55	EB
VVV 515673059596	18:07:55.9	-36:57:18.0	0.6693	0.46	15.74	15.86	15.57	15.41	15.31	EB
VVV 515673201881	18:10:11.7	-36:55:19.2	0.6127	0.66	15.88	16.03	15.76	15.56	15.50	EW
VVV 515673264133	18:11:50.1	-36:58:04.8	17.8712	0.16	15.72	15.86	15.54	15.35	15.30	EB
VVV 515673317141	18:11:53.7	-36:52:33.6	0.9669	0.29	14.51	14.62	14.38	14.21	14.16	EW
VVV 515673328256	18:12:30.7	-36:55:08.4	0.5831	0.20	14.43	14.52	14.32	14.24	14.21	EW
VVV 515680382983	18:16:30.2	-38:23:06.0	1.6508	0.35	15.70	15.72	15.76	15.81	15.83	EW
VVV 515680547234	18:15:33.8	-37:54:39.6	3.4805	0.34	15.44	15.58	15.32	15.13	15.07	EW
VVV 515680615330	18:12:42.7	-37:27:39.6	0.3659	0.26	15.33	15.46	15.18	15.00	14.91	EW
VVV 515680622640	18:13:43.2	-37:32:42.0	0.3865	0.18	15.61	15.76	15.50	15.28	15.23	EW
VVV 515680680942	18:14:36.7	-37:30:00.0	0.5997	0.16	14.95	15.07	14.83	14.66	14.61	EW
VVV 515680875793	18:14:52.0	-37:03:43.2	0.2047	0.18	15.35	15.55	15.20	14.97	14.88	EA
VVV 515690881543	18:02:24.4	-38:59:52.8	0.3891	0.39	15.25	15.36	15.10	14.88	14.82	EW
VVV 515690883735	18:04:03.3	-39:09:57.6	0.4910	0.18	14.67	14.76	14.57	14.47	14.43	EW
VVV 515691039465	18:03:19.9	-38:45:36.0	1.3439	0.42	14.39	14.52	14.26	14.08	14.02	EW
VVV 515691068640	18:05:59.2	-38:58:30.0	0.4464	0.22	13.58	13.69	13.43	13.26	13.22	EW
VVV 515691222322	18:04:16.3	-38:28:15.6	0.4262	0.56	15.79	15.91	15.65	15.46	15.40	EA
VVV 515691315050	18:09:04.5	-38:46:01.2	0.4500	0.41	15.46	15.56	15.32	15.14	15.16	EA
VVV 515691375505	18:06:17.2	-38:21:39.6	0.5737	0.17	15.05	15.15	14.97	14.82	14.77	EW
VVV 515691381843	18:05:41.2	-38:16:48.0	0.7397	0.20	15.76	15.89	15.64	15.49	15.39	EW
VVV 515691559812	18:09:06.2	-38:15:21.6	0.7275	0.15	14.62	14.74	14.48	14.30	14.25	EW
VVV 515698967529	18:13:42.7	-39:03:57.6	0.5190	0.22	14.80	14.88	14.74	14.67	14.61	EB
VVV 515698970778	18:11:17.7	-38:49:12.0	0.4505	0.44	16.21	16.33	16.08	15.91	15.89	EW
VVV 515699090050	18:13:22.3	-38:45:43.2	0.3802	0.85	14.00	14.18	13.86	13.68	13.58	EB
VVV 515699107762	18:12:43.9	-38:39:28.8	1.9066	0.17	14.06	14.19	13.93	13.71	13.65	EA
VVV 515699158314	18:11:48.9	-38:27:25.2	0.8112	0.30	14.58	14.71	14.50	14.43	14.40	EW
VVV 515699159114	18:11:21.1	-38:24:25.2	0.6083	0.23	15.49	15.61	15.35	15.21	15.15	EW
VVV 515701218814	17:58:39.6	-40:13:44.4	0.6736	0.19	13.40	13.53	13.20	12.97	12.93	EW
VVV 515705875996	18:01:08.8	-40:32:06.0	0.2071	0.18	13.67	13.78	13.49	13.31	13.26	EA
VVV 515705882538	17:59:40.8	-40:22:15.6	0.4670	0.39	15.65	15.77	15.56	15.36	15.37	EW
VVV 515705967915	18:03:40.3	-40:36:25.2	0.8621	0.32	15.57	15.70	15.40	15.22	15.17	EW
VVV 515706119055	18:04:44.4	-40:24:46.8	0.5142	0.17	14.99	15.06	14.94	14.83	14.78	EB
VVV 515706197751	18:03:02.4	-40:04:58.8	0.5144	0.31	15.34	15.45	15.16	15.00	14.93	EW
VVV 515706203313	18:03:10.3	-40:05:09.6	13.4869	0.30	15.93	15.99	15.92	15.92	15.89	EW
VVV 515706230411	18:00:53.0	-39:47:49.2	0.2005	0.22	13.41	13.56	13.21	12.95	12.94	EB
VVV 515706232080	18:04:43.4	-40:11:16.8	0.2172	0.20	13.89	13.99	13.84	13.74	13.74	EW
VVV 515706248820	18:04:03.6	-40:05:09.6	0.4042	0.24	14.87	14.97	14.69	14.54	14.48	EW

Table 1 continued

Table 1 (continued)

VVV ID	RA(J2000)	DEC(J2000)	Period	A_{K_s}	Z	Y	J	H	K_s	Class
VVV 515706291056	18:01:58.5	-39:47:13.2	3.5127	0.17	13.38	13.52	13.21	12.98	12.90	EB
VVV 515706407787	18:05:30.2	-39:54:50.4	1.3200	0.46	15.89	16.03	15.70	15.49	15.44	EB
VVV 515706508519	18:05:05.7	-39:40:12.0	1.7541	0.36	14.16	14.30	13.99	13.78	13.71	EA
VVV 515706548976	18:02:59.2	-39:22:08.4	0.7039	0.20	14.69	14.85	14.56	14.35	14.30	EW
VVV 515706571032	18:06:06.0	-39:38:27.6	0.8259	0.34	15.16	15.29	14.99	14.82	14.78	EA
VVV 515706643056	18:03:24.9	-39:12:57.6	0.3410	0.17	15.68	15.84	15.48	15.24	15.23	EW
VVV 515711751991	18:05:04.3	-40:35:31.2	0.5681	0.40	15.25	15.37	15.21	15.05	15.05	EB
VVV 515711979292	18:05:37.4	-40:07:08.4	1.0167	0.18	13.71	13.83	13.58	13.43	13.35	EW
VVV 515712262485	18:07:45.8	-39:39:39.6	0.3598	0.16	14.15	14.30	14.00	13.78	13.71	EW
VVV 515718806330	17:58:44.8	-41:38:34.8	0.5311	0.17	15.10	15.22	14.91	14.75	14.68	EW
VVV 515718867546	17:59:35.5	-41:35:49.2	0.4867	0.18	15.36	15.48	15.20	15.01	14.97	EW
VVV 515718947320	18:00:13.9	-41:29:31.2	0.5321	0.17	14.71	14.85	14.53	14.32	14.25	EW
VVV 515719214581	18:01:03.8	-41:00:43.2	2.3970	0.20	15.23	15.38	15.11	14.95	14.90	EW
VVV 515719268802	18:01:07.4	-40:54:21.6	0.6073	0.17	14.85	15.00	14.67	14.41	14.34	EW
VVV 515719330993	18:01:17.2	-40:47:24.0	0.6150	0.18	14.20	14.32	14.00	13.78	13.71	EB
VVV 515719401200	17:59:41.5	-40:29:06.0	0.4648	0.23	14.36	14.51	14.19	13.97	13.89	EW
VVV 515723080317	18:02:43.4	-42:05:02.4	0.4644	0.28	13.39	13.49	13.27	13.16	13.10	EA
VVV 515723113577	18:05:34.8	-42:16:48.0	0.6526	0.32	14.42	14.52	14.30	14.15	14.11	EW
VVV 515723223326	18:02:34.0	-41:43:12.0	0.4815	0.30	13.98	14.08	13.88	13.72	13.66	EB
VVV 515723445466	18:04:11.5	-41:19:51.6	1.4838	0.34	14.68	14.79	14.56	14.40	14.33	EA

^aThe complete parameters: VVV ID, right ascension (J2000), declination (J2000), period (days), amplitude of K_s magnitude, $ZYKHK_s$ magnitudes and type of eclipsing binary.

Table 2. Complete Parameters for the Second Category of Eclipsing Binaries

VVV ID	RA(J2000)	DEC(J2000)	Period	A_{K_s}	Z	Y	J	H	K_s	Class
VVV 515455684844	18:39:58.3	-25:03:36.0	0.1542	0.22	15.91	16.06	15.69	15.55	15.42	EB
VVV 515455868670	18:40:48.9	-24:49:37.2	0.1043	0.20	15.95	16.10	15.75	15.55	15.52	EW
VVV 515455933928	18:39:48.9	-24:35:56.4	0.1157	0.21	16.20	16.37	15.98	15.72	15.76	EW
VVV 515456085853	18:38:39.1	-24:11:38.4	0.2052	0.31	15.41	15.59	15.16	14.90	14.79	EA
VVV 515456440625	18:39:44.6	-23:38:24.0	0.1997	0.25	15.34	15.52	15.09	14.85	14.74	EW
VVV 515463134581	18:43:55.4	-25:19:58.8	0.1374	0.19	15.61	15.78	15.43	15.32	15.20	EW
VVV 515463225981	18:42:07.9	-24:57:36.0	0.1826	0.26	15.32	15.46	15.19	15.09	15.05	EA
VVV 515478514260	18:36:37.4	-26:13:01.2	0.1662	0.15	15.51	15.69	15.36	15.21	15.16	EB
VVV 515479052288	18:36:22.3	-25:14:31.2	0.1112	0.19	15.88	16.05	15.64	15.45	15.36	EB
VVV 515479171894	18:39:00.9	-25:19:22.8	0.1453	0.17	15.53	15.70	15.41	15.25	15.22	EB
VVV 515479177449	18:37:27.1	-25:08:34.8	0.1163	0.53	16.48	16.67	16.35	16.10	16.22	EW
VVV 515485889422	18:41:38.4	-26:32:49.2	0.2010	0.20	15.81	15.96	15.62	15.48	15.37	EB
VVV 515485958127	18:40:04.5	-26:14:49.2	0.4994	0.84	15.73	15.95	15.55	15.38	15.31	EB
VVV 515502887985	18:32:35.2	-27:03:57.6	0.3325	0.16	15.59	15.74	15.43	15.25	15.21	EW
VVV 515503027404	18:33:09.6	-26:47:16.8	1.1476	0.74	16.00	16.11	15.80	15.64	15.55	EA
VVV 515503126084	18:35:54.4	-26:50:52.8	1.6274	0.19	14.73	14.90	14.54	14.33	14.26	EB
VVV 515503129050	18:33:38.8	-26:35:38.4	0.1217	0.32	15.84	15.96	15.65	15.49	15.40	EB
VVV 515509272322	18:39:11.7	-28:06:46.8	0.1328	0.36	16.04	16.15	16.02	16.02	16.01	EW
VVV 515509278310	18:35:57.1	-27:45:00.0	0.2819	0.16	14.77	14.91	14.62	14.45	14.39	EW
VVV 515509304509	18:37:33.6	-27:52:37.2	8.0162	0.17	15.60	15.78	15.42	15.25	15.19	EB
VVV 515509403573	18:38:48.9	-27:50:24.0	0.1047	0.24	15.94	16.09	15.78	15.63	15.55	EB
VVV 515509410203	18:39:10.3	-27:52:01.2	0.1323	0.47	16.53	16.62	16.46	16.30	16.38	EW
VVV 515509663612	18:41:36.7	-27:41:06.0	0.1219	0.18	15.69	15.85	15.52	15.36	15.22	EW

Table 2 continued

Table 2 (continued)

VVV ID	RA(J2000)	DEC(J2000)	Period	A_{K_s}	Z	Y	J	H	K_s	Class
VVV 515509869037	18:41:32.4	-27:18:46.8	1.0061	0.17	14.70	14.86	14.55	14.40	14.33	EW
VVV 515524607103	18:30:48.7	-28:50:09.6	9.3646	0.32	16.19	16.35	16.00	15.85	15.79	EW
VVV 515524666001	18:32:12.9	-28:52:58.8	0.1206	0.16	15.37	15.51	15.23	15.10	15.05	EB
VVV 515524725961	18:30:37.9	-28:36:32.4	0.1567	0.16	15.29	15.43	15.13	14.99	14.94	EB
VVV 515524735722	18:30:55.4	-28:36:57.6	0.1460	0.21	15.73	15.84	15.62	15.58	15.48	EW
VVV 515525259156	18:34:04.8	-28:01:15.6	0.1727	0.25	15.73	15.84	15.67	15.58	15.55	EW
VVV 515525330846	18:34:42.9	-27:57:21.6	0.2803	0.22	15.97	16.13	15.77	15.59	15.51	EB
VVV 515525356127	18:33:53.4	-27:49:12.0	0.1054	0.41	16.51	16.64	16.46	16.37	16.32	EW
VVV 515532782662	18:34:52.8	-29:19:40.8	0.1320	0.28	16.08	16.22	15.93	15.79	15.71	EB
VVV 515532855488	18:36:00.2	-29:20:24.0	0.1293	0.21	13.60	13.76	13.41	13.14	13.07	EB
VVV 515532865640	18:36:32.4	-29:23:02.4	0.1767	0.28	16.01	16.12	15.95	15.87	15.88	EB
VVV 515532908547	18:37:43.6	-29:26:31.2	0.1130	0.19	14.17	14.27	14.00	13.79	13.75	EB
VVV 515547271786	18:27:21.1	-29:13:48.0	0.1910	0.54	16.41	16.48	16.38	16.30	16.32	EW
VVV 515556675040	18:35:36.2	-30:12:32.4	0.1530	0.17	15.19	15.31	15.07	14.95	14.90	EW
VVV 515556719489	18:36:10.3	-30:11:16.8	0.1862	0.20	15.05	15.17	14.98	14.90	14.87	EW
VVV 515557033917	18:33:50.6	-29:20:56.4	0.1078	0.42	16.57	16.71	16.58	16.56	16.54	EW
VVV 515568514119	18:23:06.4	-31:04:37.2	0.1613	0.81	16.34	16.30	16.32	16.36	16.29	EB
VVV 515568557126	18:26:19.6	-31:21:07.2	0.1114	0.25	16.24	16.36	16.10	15.94	15.91	EW
VVV 515568632532	18:24:41.0	-31:03:28.8	0.1017	0.17	14.09	14.09	13.96	13.81	13.76	EW
VVV 515568722837	18:27:25.6	-31:12:18.0	5.8910	0.37	15.97	16.00	15.83	15.70	15.68	EB
VVV 515577520620	18:30:07.6	-31:51:14.4	1.3347	0.19	14.52	14.65	14.43	14.28	14.25	EW
VVV 515577532611	18:31:17.7	-31:56:42.0	0.8757	0.18	15.21	15.31	15.14	15.10	15.05	EW
VVV 515577618069	18:32:06.0	-31:49:44.4	0.1752	0.18	15.67	15.68	15.65	15.65	15.62	EW
VVV 515577688955	18:32:39.1	-31:43:15.6	0.1007	0.67	16.48	16.62	16.54	16.40	16.53	EB
VVV 515577709444	18:32:36.4	-31:40:12.0	0.3293	0.41	16.22	16.24	16.18	16.15	16.10	EW
VVV 515577954723	18:31:45.3	-31:00:54.0	0.1994	0.22	15.62	15.77	15.47	15.31	15.25	EW
VVV 515589502665	18:20:24.2	-32:37:33.6	0.1135	0.19	15.72	15.84	15.54	15.35	15.32	EW
VVV 515589619696	18:21:04.5	-32:26:24.0	0.1004	0.29	15.60	15.68	15.56	15.53	15.53	EW
VVV 515589691165	18:20:26.1	-32:12:07.2	9.6299	0.17	15.55	15.70	15.38	15.25	15.18	EB
VVV 515589758665	18:23:25.9	-32:22:04.8	0.1170	0.48	15.34	15.49	15.15	14.94	14.89	EA
VVV 515589874419	18:22:04.0	-31:57:14.4	0.2610	0.25	15.76	15.95	15.63	15.43	15.40	EW
VVV 515590009973	18:23:11.0	-31:46:15.6	0.1079	0.18	15.61	15.76	15.44	15.32	15.23	EW
VVV 515598803695	18:26:21.1	-32:24:57.6	0.1979	0.65	16.11	16.24	16.05	15.91	15.86	EB
VVV 515612097220	18:20:31.9	-34:16:33.6	0.3882	0.22	15.29	15.43	15.11	14.88	14.79	EW
VVV 515612715112	18:19:07.2	-33:09:03.6	1.8403	0.16	15.25	15.37	15.11	14.96	14.91	EB
VVV 515620104648	18:24:02.8	-34:15:28.8	0.1817	0.31	16.12	16.14	16.10	16.06	16.09	EW
VVV 515620196397	18:23:51.1	-34:06:03.6	0.1198	0.38	15.96	15.93	15.99	16.08	16.05	EW
VVV 515620345157	18:25:43.4	-33:59:20.4	0.1165	0.22	16.06	15.96	16.06	16.06	16.10	EW
VVV 515620607952	18:26:41.7	-33:36:18.0	1.2112	0.16	15.18	15.31	15.06	14.92	14.84	EW
VVV 515634468753	18:13:04.0	-35:10:58.8	0.1852	0.24	16.09	16.24	15.94	15.76	15.74	EW
VVV 515634479296	18:16:45.6	-35:33:10.8	0.2989	0.58	13.62	13.74	13.44	13.26	13.18	EW
VVV 515634842456	18:15:37.4	-34:48:57.6	0.1643	0.20	14.17	14.34	14.02	13.80	13.74	EB
VVV 515635045816	18:15:13.4	-34:25:37.2	0.5882	0.17	14.74	14.86	14.64	14.53	14.43	EA
VVV 515641053957	18:20:03.1	-35:24:28.8	0.1648	0.20	15.40	15.52	15.30	15.20	15.19	EB
VVV 515641129529	18:20:59.7	-35:21:32.4	0.1163	0.20	15.62	15.70	15.51	15.43	15.40	EW
VVV 515641189156	18:22:04.3	-35:21:18.0	0.3316	0.25	16.05	16.15	15.97	15.90	15.88	EB
VVV 515641514958	18:23:23.5	-34:51:25.2	0.1185	0.16	14.28	14.38	14.16	14.00	13.97	EW
VVV 515641537845	18:24:18.2	-34:54:07.2	0.1004	0.18	15.61	15.65	15.61	15.65	15.55	EW
VVV 515655508764	18:13:22.3	-36:53:34.8	0.1374	0.92	16.01	16.14	15.96	15.88	15.88	EB
VVV 515655641620	18:12:31.2	-36:35:31.2	0.1650	0.32	16.02	16.07	15.97	15.97	15.92	EB
VVV 515655889118	18:14:47.0	-36:26:16.8	0.1582	0.16	15.48	15.58	15.32	15.12	15.12	EA
VVV 515655958303	18:13:02.1	-36:08:52.8	0.1781	0.49	15.89	15.95	15.81	15.67	15.64	EA
VVV 515656307969	18:12:18.0	-35:30:46.8	0.1029	0.29	15.86	16.00	15.73	15.63	15.59	EB
VVV 515660511022	18:19:18.0	-37:01:08.4	0.3995	0.31	15.41	15.49	15.39	15.41	15.39	EW

Table 2 continued

Table 2 (continued)

VVV ID	RA(J2000)	DEC(J2000)	Period	A_{K_s}	Z	Y	J	H	K_s	Class
VVV 515660564477	18:15:51.6	-36:34:37.2	1.3153	0.74	15.76	15.71	15.62	15.42	15.38	EB
VVV 515660666659	18:17:39.1	-36:32:34.8	0.1232	0.32	15.96	16.01	15.94	15.97	15.87	EB
VVV 515660826021	18:19:03.8	-36:21:54.0	0.1451	0.84	16.21	16.26	16.17	16.10	16.11	EA
VVV 515660831491	18:19:42.9	-36:25:12.0	0.1307	0.39	16.38	16.48	16.35	16.31	16.29	EW
VVV 515672740485	18:08:05.7	-37:35:31.2	0.2240	0.21	14.86	14.95	14.75	14.63	14.61	EA
VVV 515673176777	18:09:11.5	-36:51:50.4	0.1340	0.20	15.71	15.74	15.68	15.61	15.69	EB
VVV 515673192054	18:11:14.6	-37:02:56.4	0.1010	0.38	16.30	16.35	16.28	16.28	16.23	EW
VVV 515673300569	18:09:49.9	-36:41:31.2	0.1810	0.23	15.75	15.85	15.71	15.63	15.63	EB
VVV 515673315465	18:12:25.2	-36:56:13.2	0.1233	0.15	14.55	14.73	14.38	14.10	14.05	EW
VVV 515680316550	18:12:26.6	-38:07:55.2	0.1531	0.39	16.15	16.13	16.16	16.25	16.23	EB
VVV 515680320514	18:13:58.8	-38:16:37.2	0.1114	0.39	15.98	16.03	15.98	16.00	15.93	EW
VVV 515680617803	18:15:34.0	-37:44:34.8	0.1217	0.31	16.21	16.23	16.24	16.29	16.22	EW
VVV 515690911790	18:03:26.4	-39:02:24.0	0.2505	0.24	15.48	15.55	15.45	15.42	15.41	EW
VVV 515691005248	18:06:29.0	-39:09:25.2	0.1603	0.17	15.84	15.92	15.74	15.66	15.58	EW
VVV 515698868428	18:09:30.4	-38:52:01.2	4.2039	0.51	16.45	16.57	16.38	16.20	16.25	EW
VVV 515711628328	18:06:12.0	-40:59:31.2	0.1470	0.24	15.87	15.98	15.73	15.58	15.55	EW
VVV 515711722950	18:05:23.5	-40:41:16.8	0.2466	0.37	16.22	16.40	16.08	15.90	15.93	EW
VVV 515711744139	18:07:08.8	-40:49:01.2	0.1502	0.33	16.15	16.22	16.17	16.20	16.28	EB
VVV 515711803436	18:05:40.5	-40:31:48.0	0.1175	0.22	14.67	14.72	14.70	14.74	14.70	EB
VVV 515711955921	18:06:59.7	-40:18:46.8	0.1015	0.15	15.51	15.61	15.40	15.30	15.28	EW
VVV 515712020864	18:06:36.4	-40:07:08.4	1.0328	0.30	16.27	16.38	16.14	16.05	15.97	EW
VVV 515712111979	18:07:31.9	-40:00:14.4	0.1715	0.43	15.24	15.32	15.18	15.09	15.05	EA
VVV 515718680805	17:57:28.3	-41:47:02.4	0.1571	0.15	14.96	15.08	14.81	14.66	14.62	EB
VVV 515718779923	17:57:21.1	-41:33:18.0	0.1187	0.28	15.92	16.04	15.80	15.67	15.66	EW
VVV 515718932470	17:59:40.8	-41:28:58.8	0.1247	0.63	16.31	16.31	16.33	16.39	16.41	EW
VVV 515723095125	18:01:02.8	-41:52:48.0	0.2873	0.56	13.70	13.82	13.53	13.32	13.28	EA
VVV 515723223326	18:02:34.0	-41:43:12.0	0.2407	0.30	13.98	14.08	13.88	13.72	13.66	EA

^aThe complete parameters: VVV ID, right ascension (J2000), declination (J2000), period (days), amplitude of K_s magnitude, $ZYKHK_s$ magnitudes and type of eclipsing binary.

Table 3. RR Lyrae Stars in our Sample.

VVV ID	VVV ID <i>Gran et al. (2016)</i>	RA(J2000)	DEC(J2000)	Period	Amp K_s	Z	Y	J	H	K_s
VVV 515706039923	J180039.53-400902.4	18:00:39.6	-40:09:03.6	0.6497	0.40	14.14	14.32	14.00	13.79	13.73
VVV 515673239493	J180949.72-364838.9	18:09:49.6	-36:48:39.6	0.5354	0.41	14.01	14.18	13.90	13.76	13.68
VVV 515672602244	J180958.42-380307.7	18:09:58.3	-38:03:07.2	0.5230	0.32	14.76	14.86	14.61	14.48	14.41
VVV 515698929724	J181011.78-384805.0	18:10:11.7	-38:48:03.6	0.6101	0.25	14.63	14.74	14.49	14.32	14.22
VVV 515656519651	J181418.96-352242.8	18:14:18.9	-35:22:44.4	0.3964	0.30	14.49	14.64	14.35	14.17	14.08
VVV 515598433507	J182748.94-332826.0	18:27:48.9	-33:28:26.4	0.5406	0.49	14.83	15.02	14.69	14.47	14.39
VVV 515533139402	J183758.88-290835.4	18:37:58.8	-29:08:34.8	0.5395	0.45	15.04	15.13	14.85	14.58	14.50
VVV 515705907121		17:59:59.2	-40:21:00.0	0.6415	0.29	14.85	14.97	14.70	14.51	14.40
VVV 515655923198		18:14:50.4	-36:23:27.6	0.4511	0.29	15.93	16.08	15.77	15.57	15.53
VVV 515598807255		18:26:03.6	-32:22:55.2	0.4550	0.42	14.86	15.01	14.71	14.57	14.47
VVV 515533825718		18:38:25.2	-28:11:27.6	0.3488	0.19	15.19	15.33	15.00	14.84	14.76
VVV 515456403764		18:41:49.9	-23:56:45.6	0.6272	0.24	14.72	14.90	14.48	14.18	14.11

^aThe complete parameters: VVV ID, right ascension (J2000), declination (J2000), period (days), amplitude of K_s magnitude and $ZYKHK_s$ magnitudes.

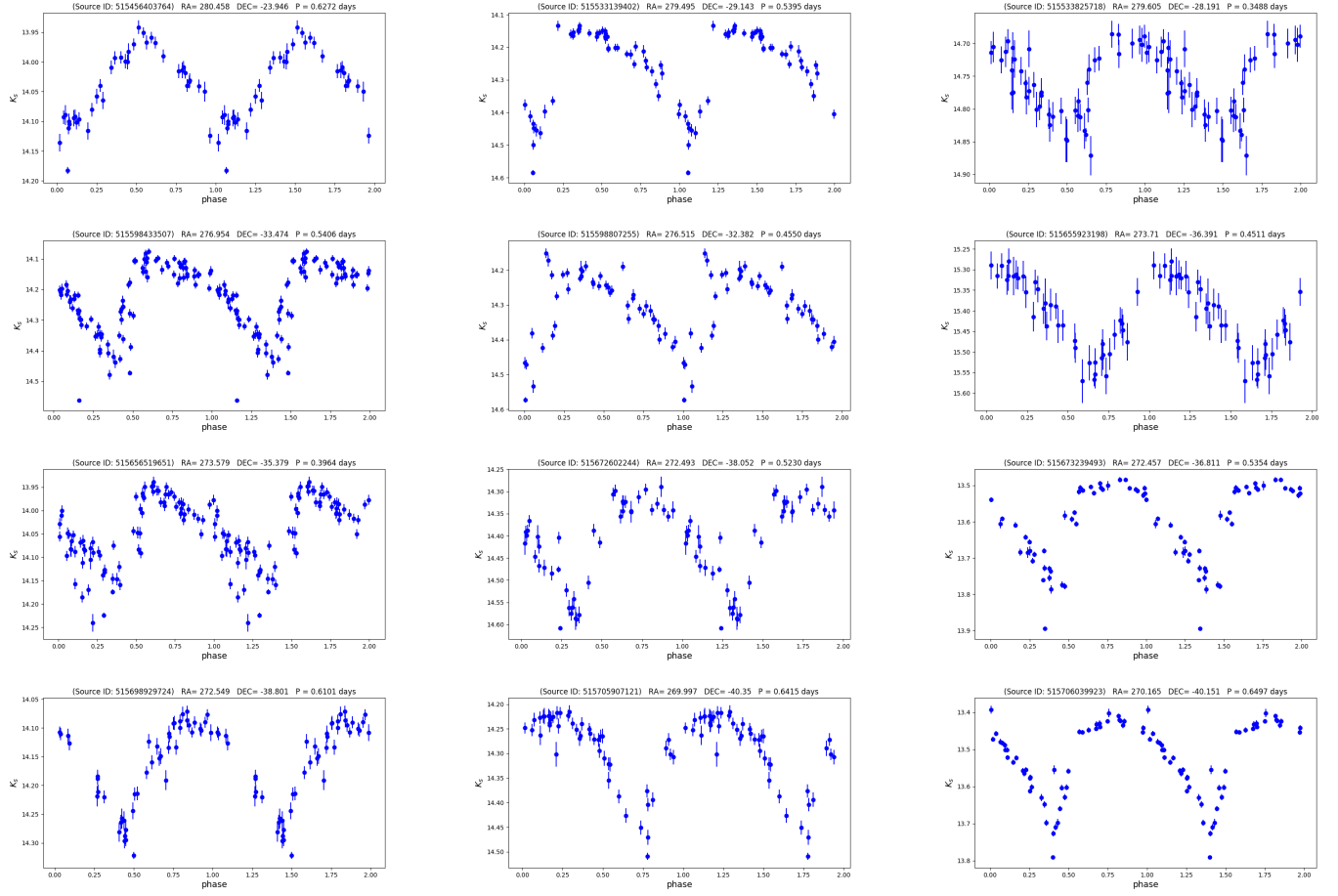


Figure 17. RR Lyrae light curves found in our sample.

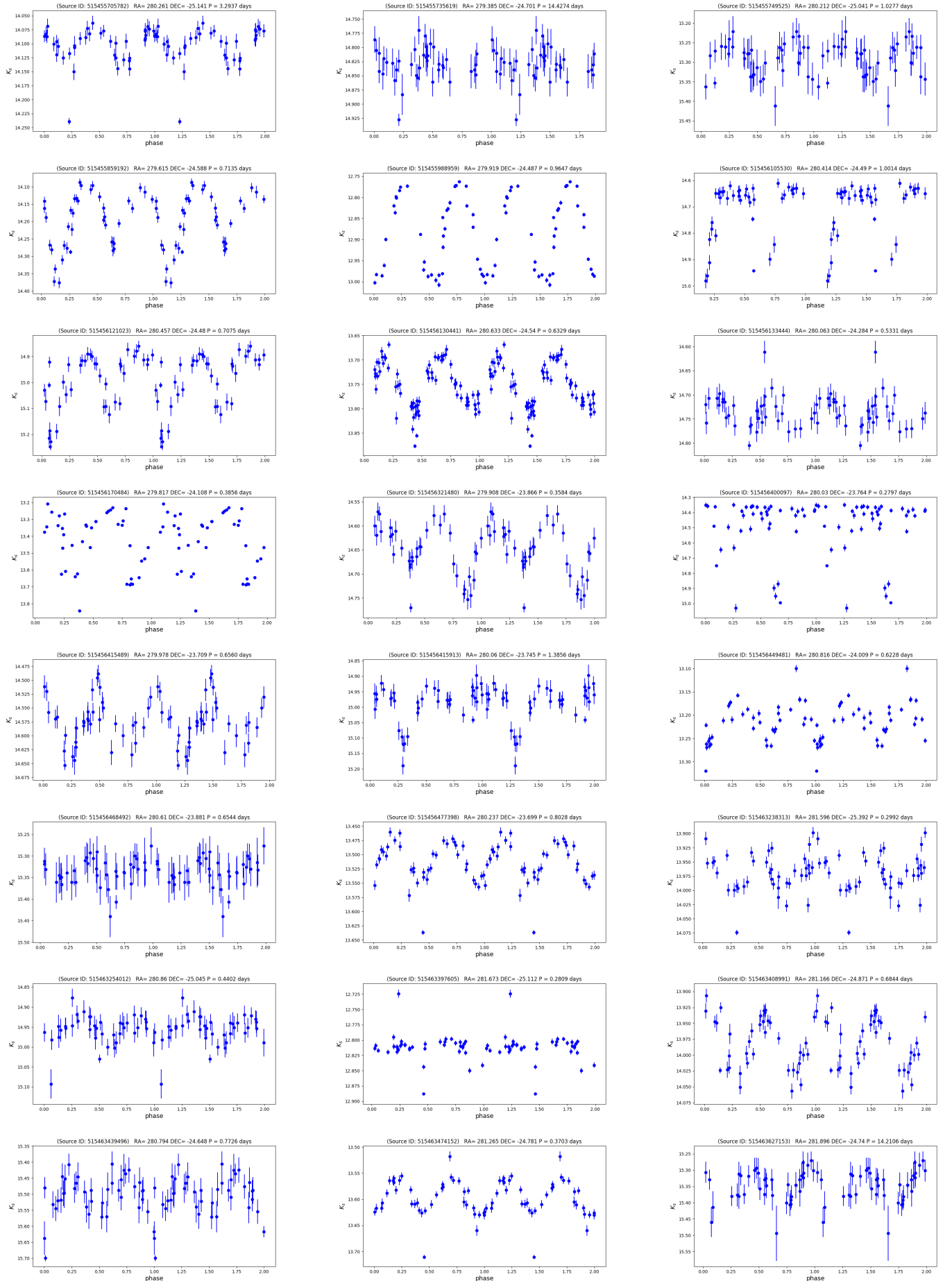


Figure 18. BHB stars light curves corresponding to 1^{st} category eclipsing binaries.

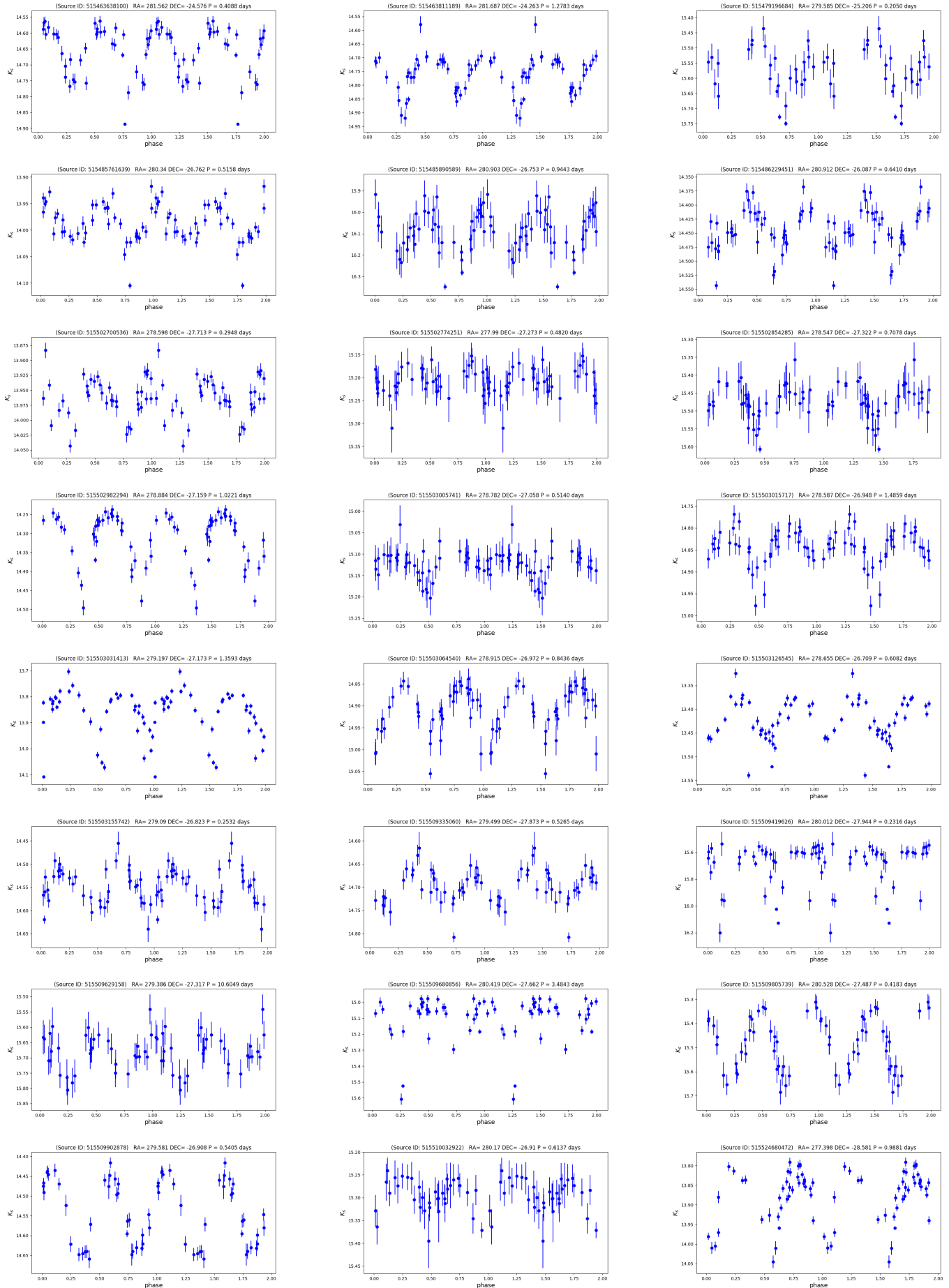


Figure 19. BHB stars light curves corresponding to 1^{st} category eclipsing binaries.

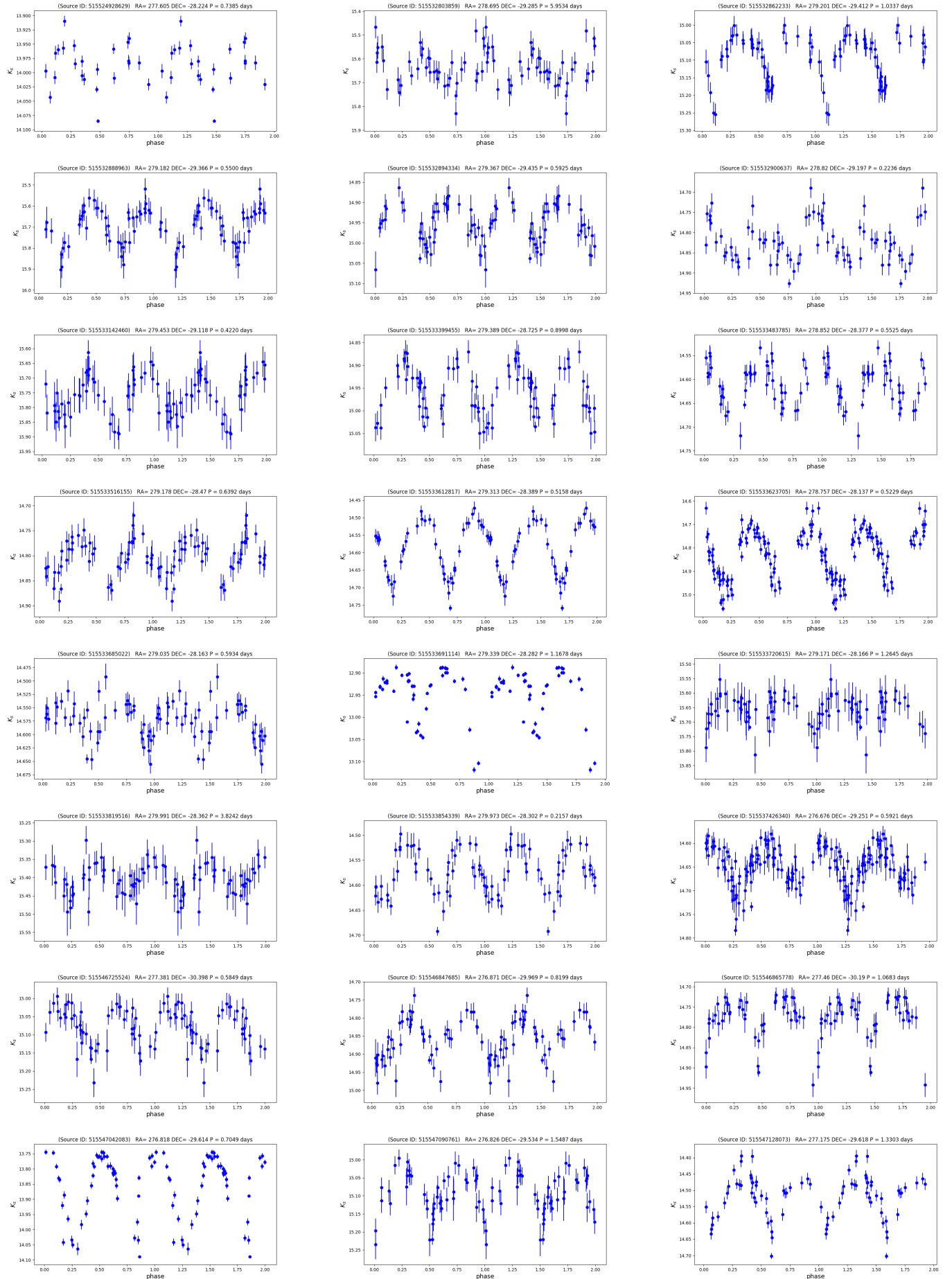


Figure 20. BHB stars light curves corresponding to 1^{st} category eclipsing binaries.

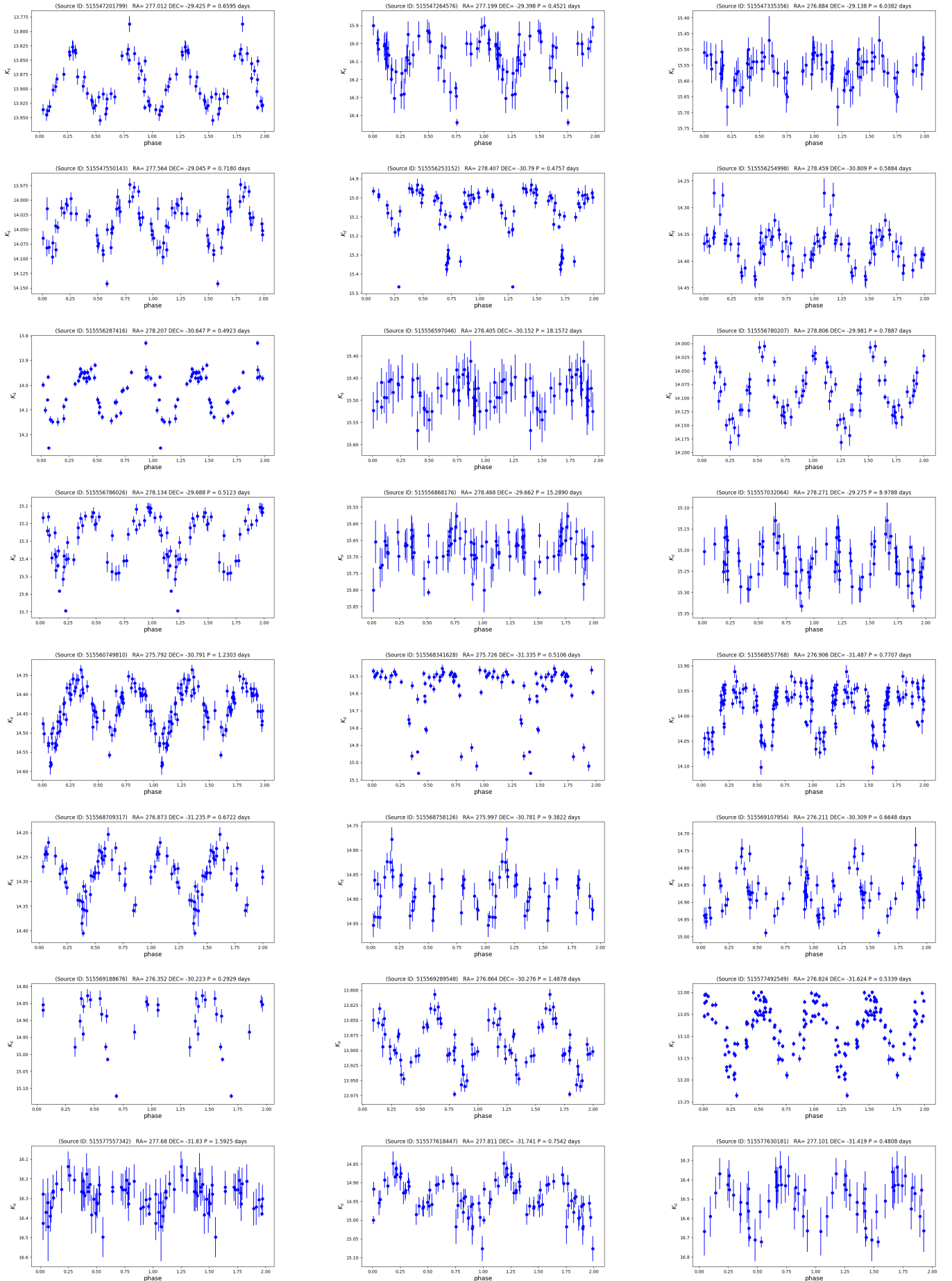


Figure 21. BHB stars light curves corresponding to 1^{st} category eclipsing binaries.

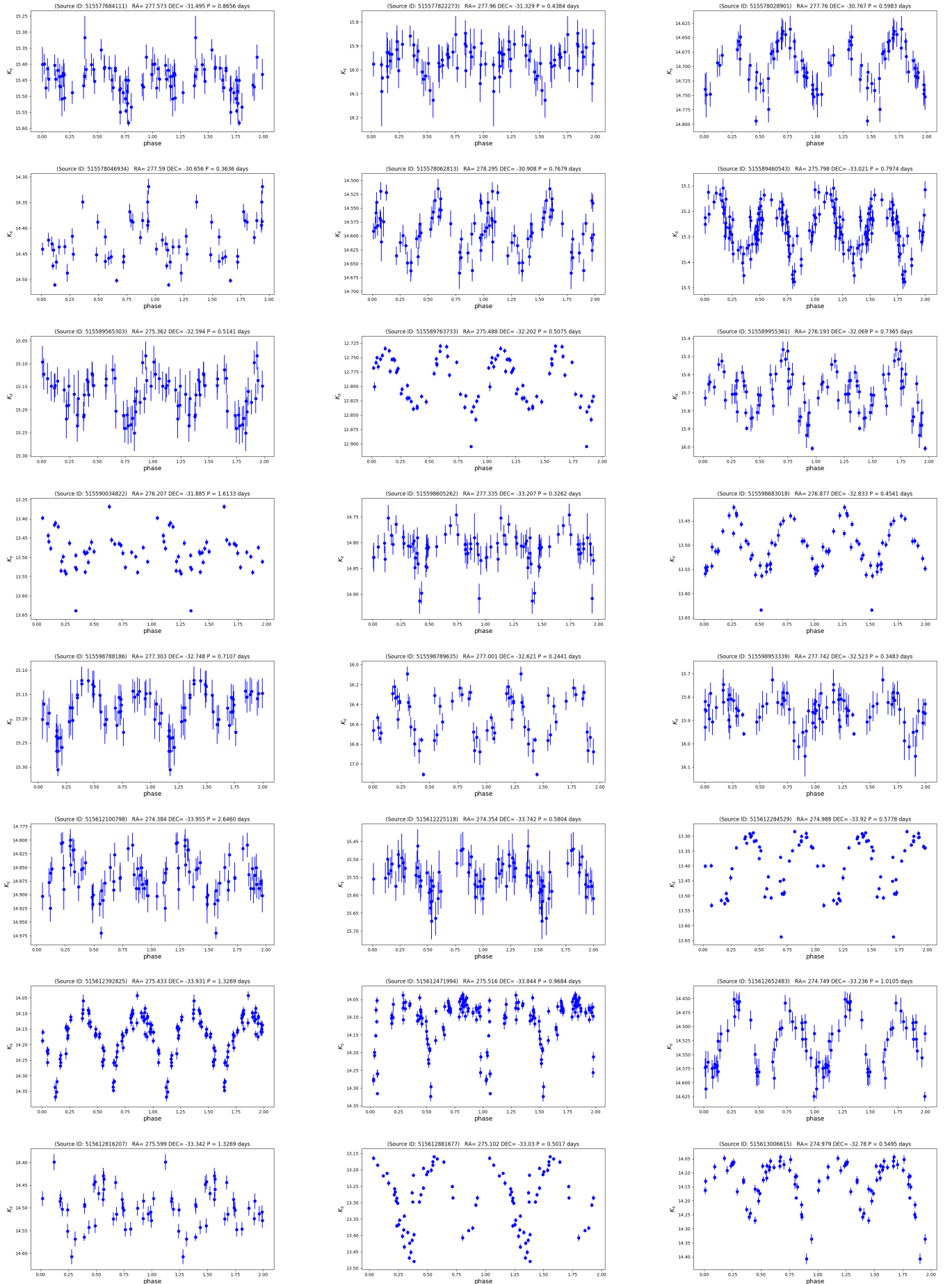


Figure 22. BHB stars light curves corresponding to 1st category eclipsing binaries.

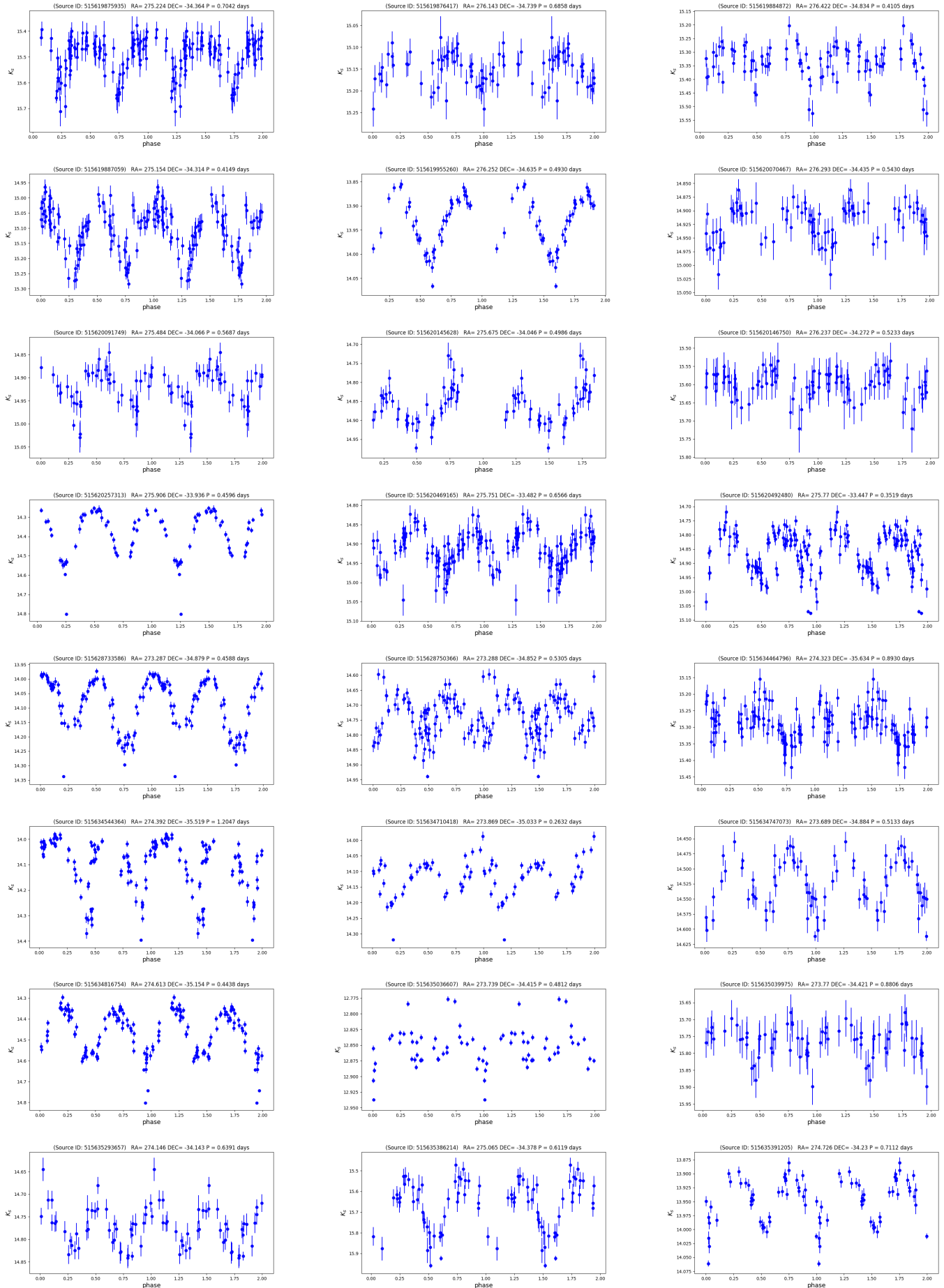


Figure 23. BHB stars light curves corresponding to 1st category eclipsing binaries.

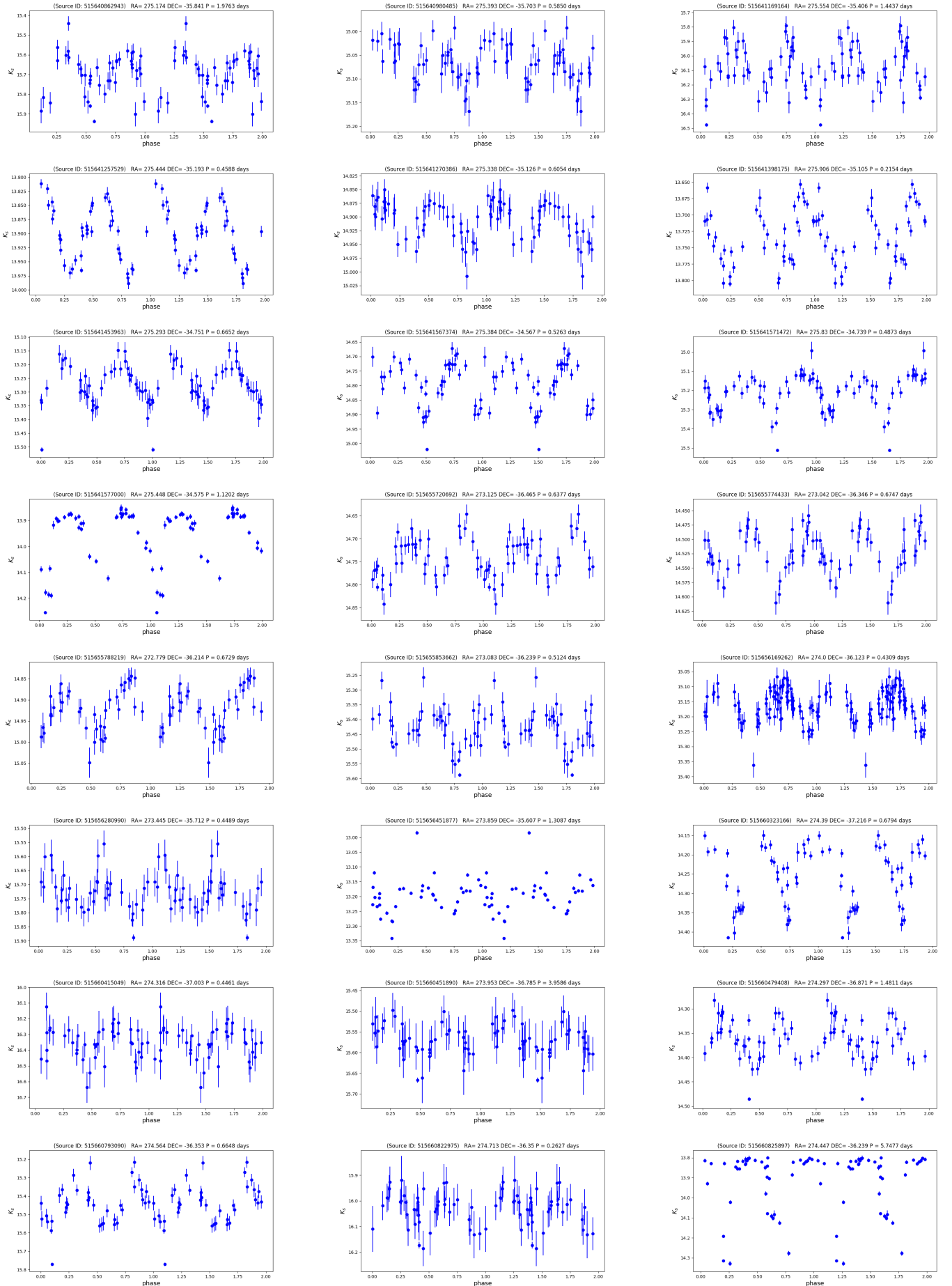


Figure 24. BHB stars light curves corresponding to 1^{st} category eclipsing binaries.

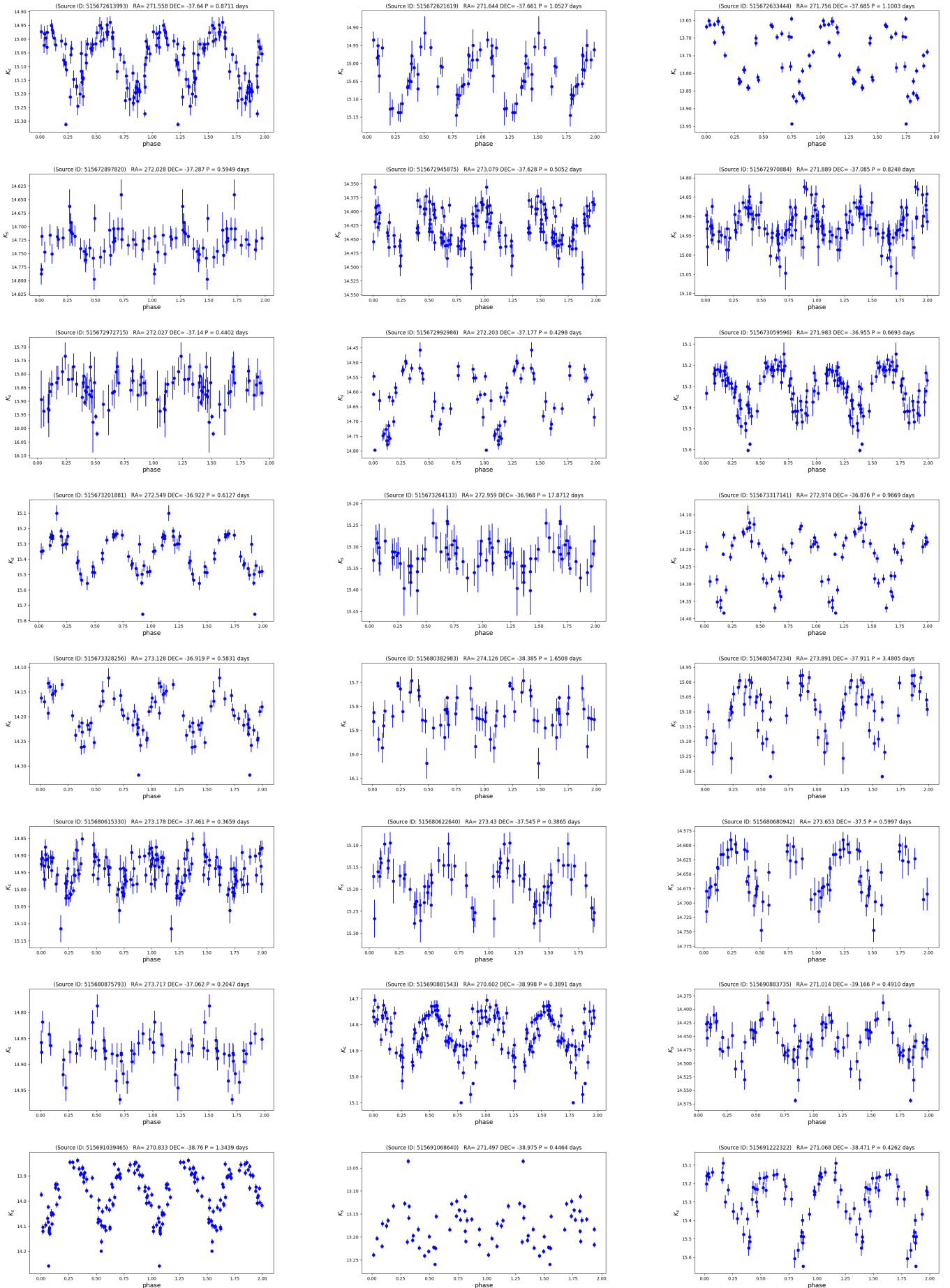


Figure 25. BHB stars light curves corresponding to 1^{st} category eclipsing binaries.

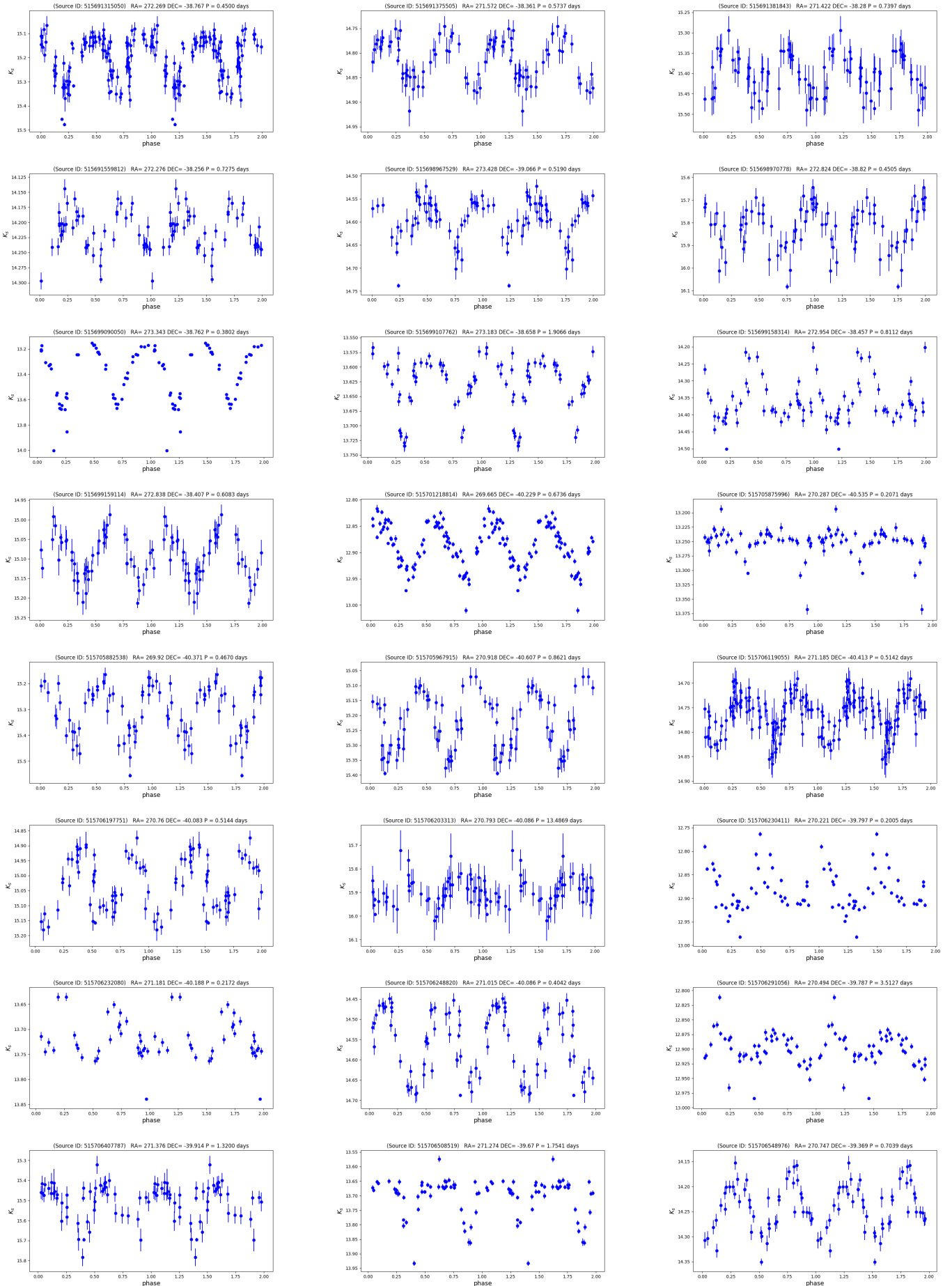


Figure 26. BHB stars light curves corresponding to 1st category eclipsing binaries.

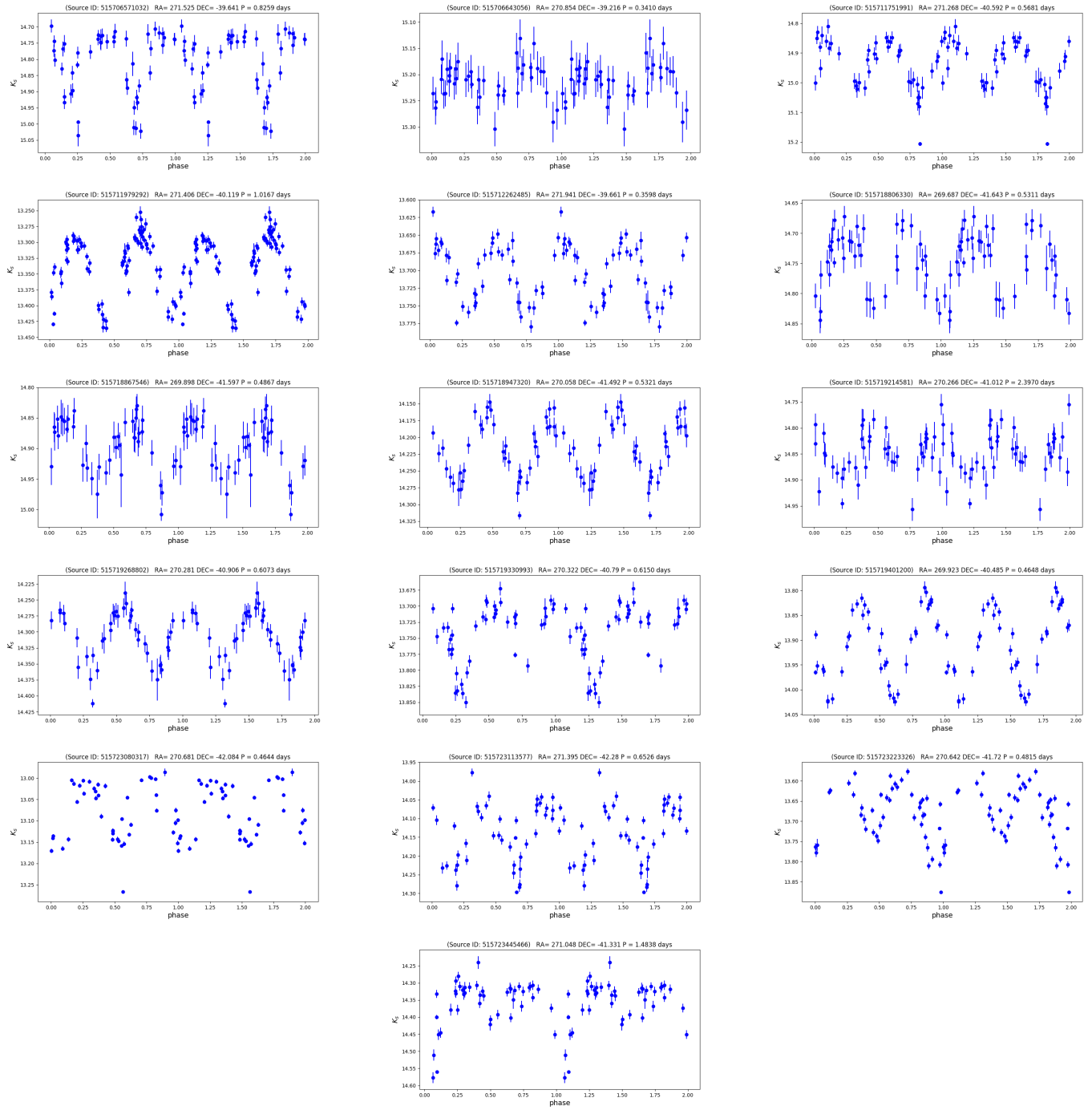


Figure 27. BHB stars light curves corresponding to 1st category eclipsing binaries.

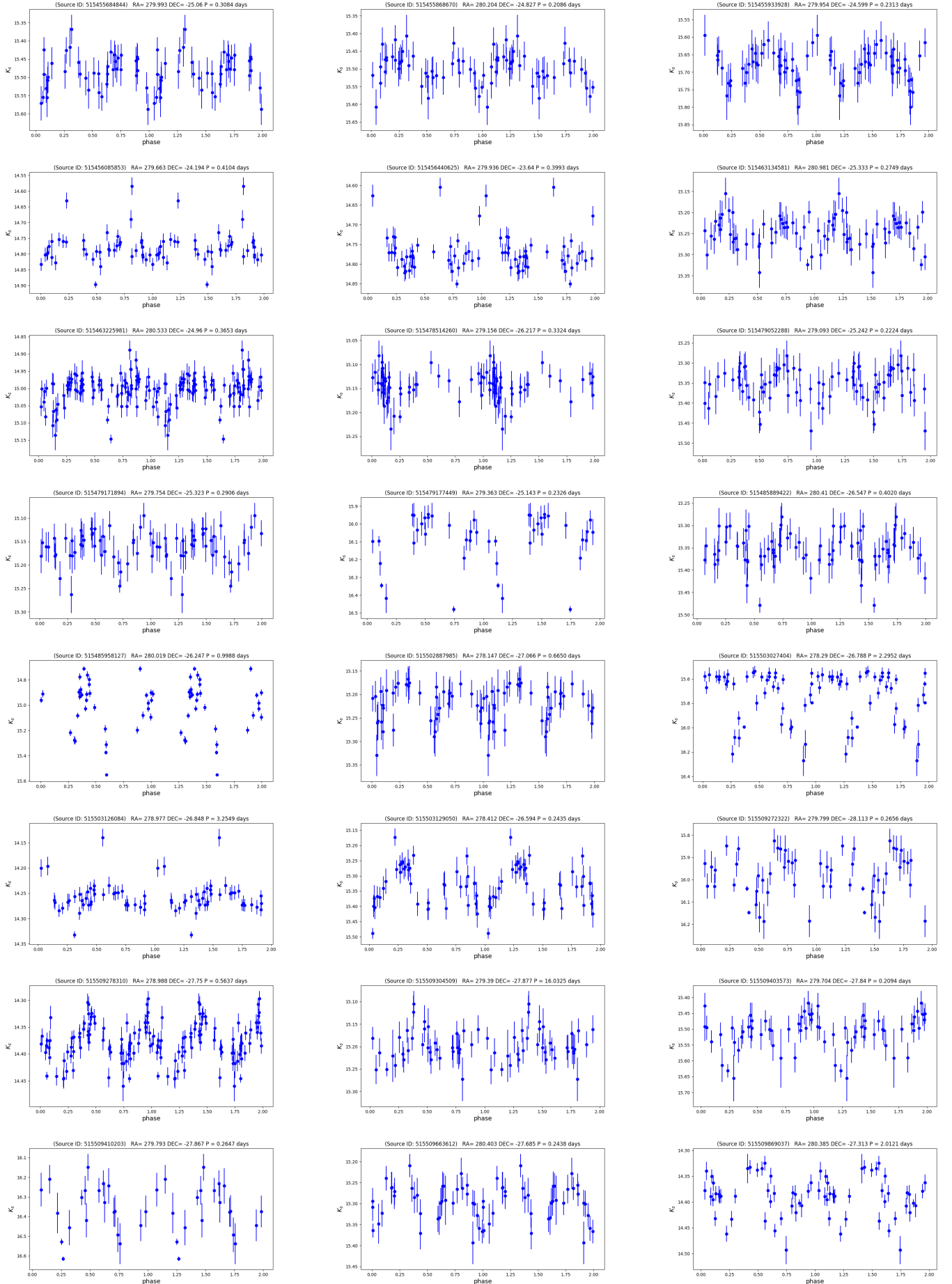


Figure 28. BHB stars light curves corresponding to 2nd category eclipsing binaries.

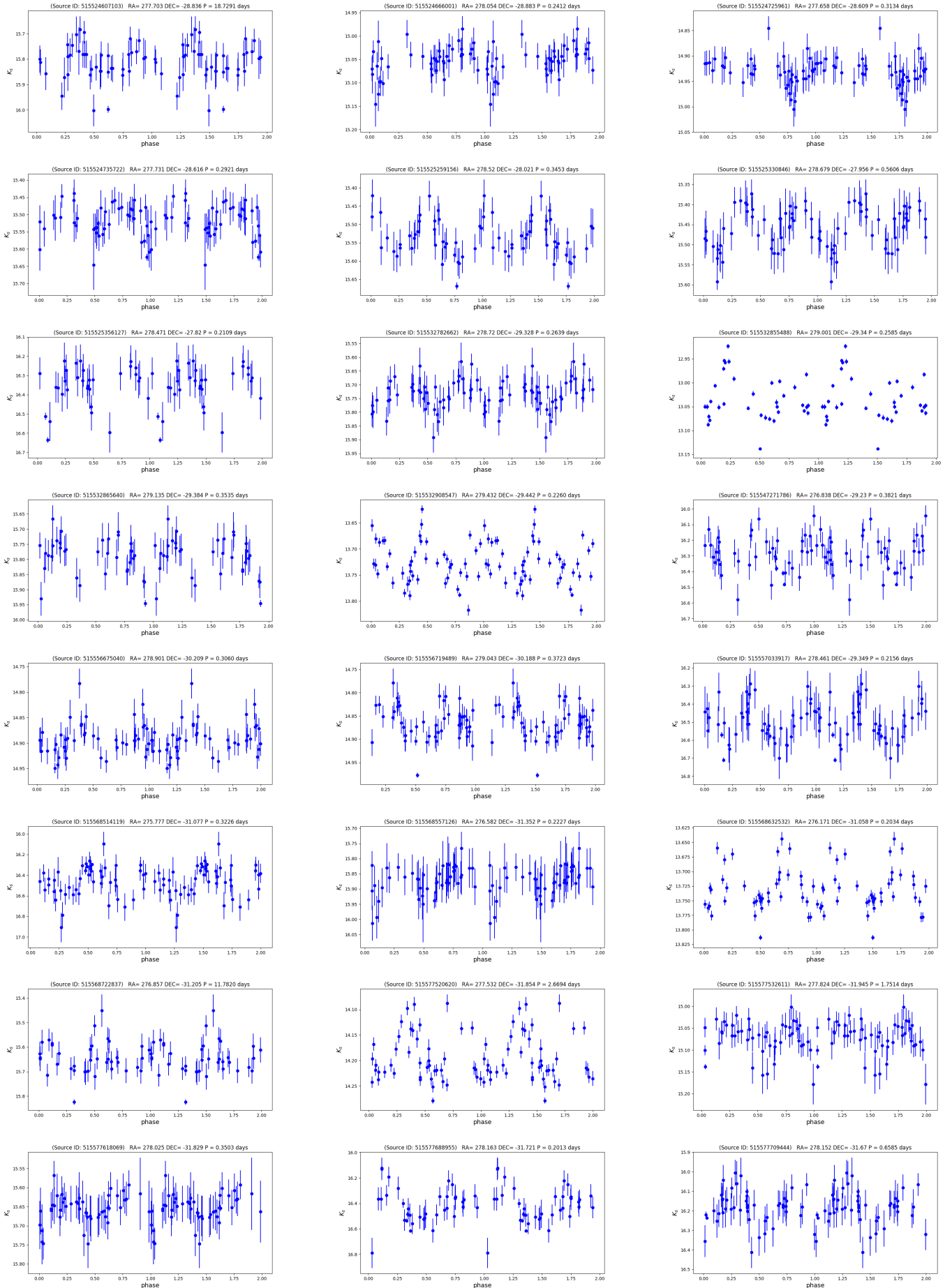


Figure 29. BHB stars light curves corresponding to 2^{nd} category eclipsing binaries.

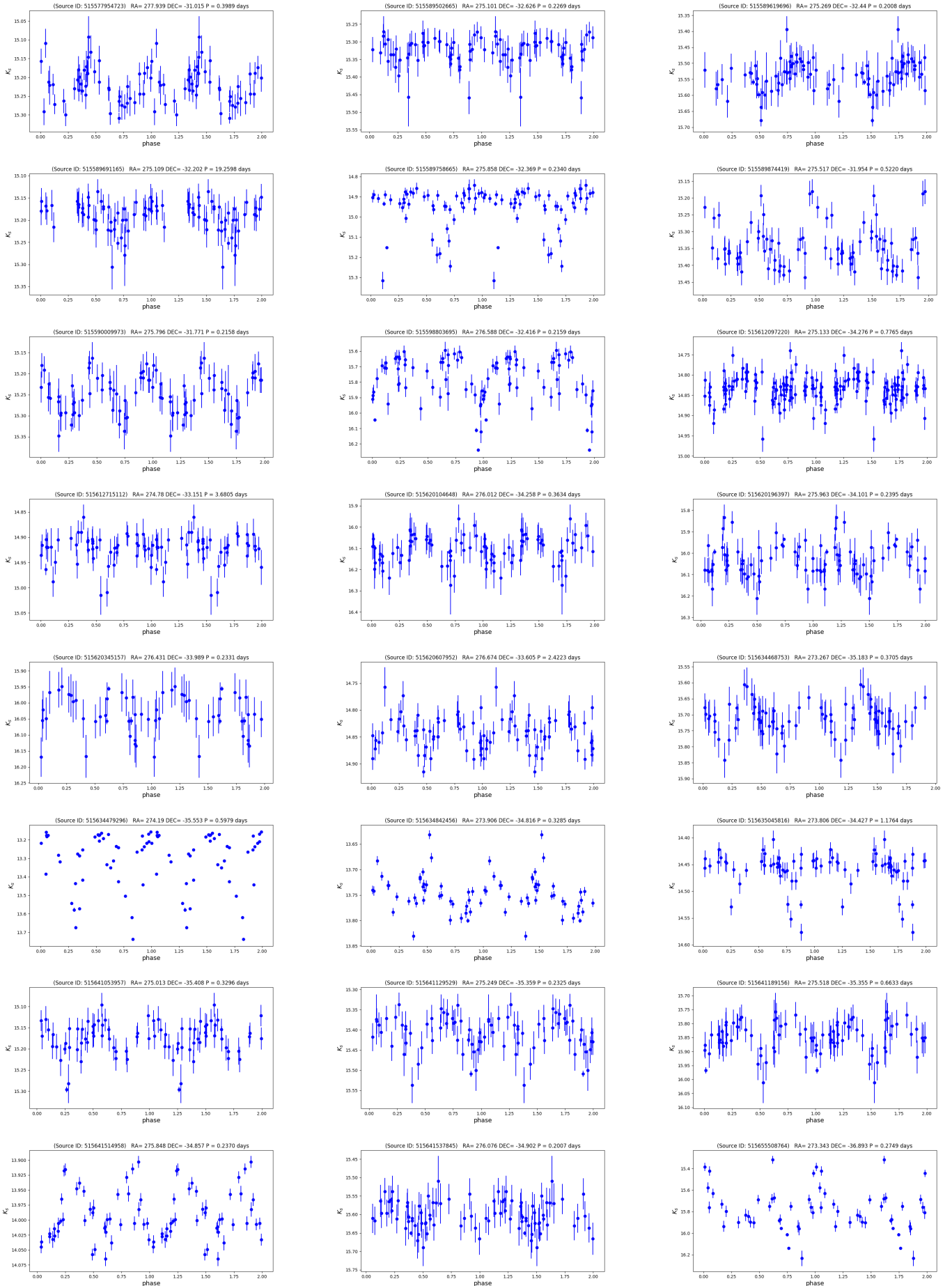


Figure 30. BHB stars light curves corresponding to 2^{nd} category eclipsing binaries.

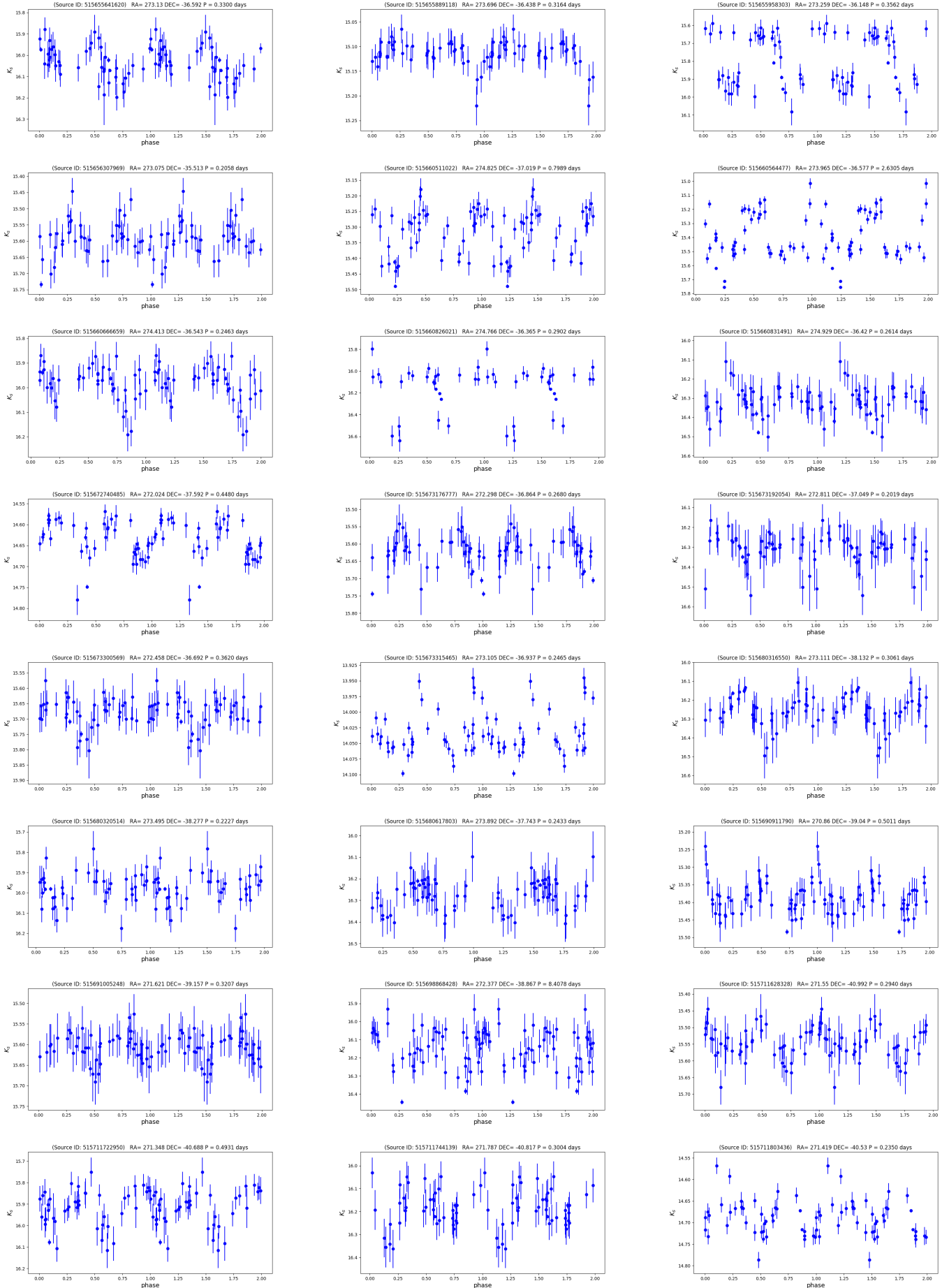


Figure 31. BHB stars light curves corresponding to 2^{nd} category eclipsing binaries.

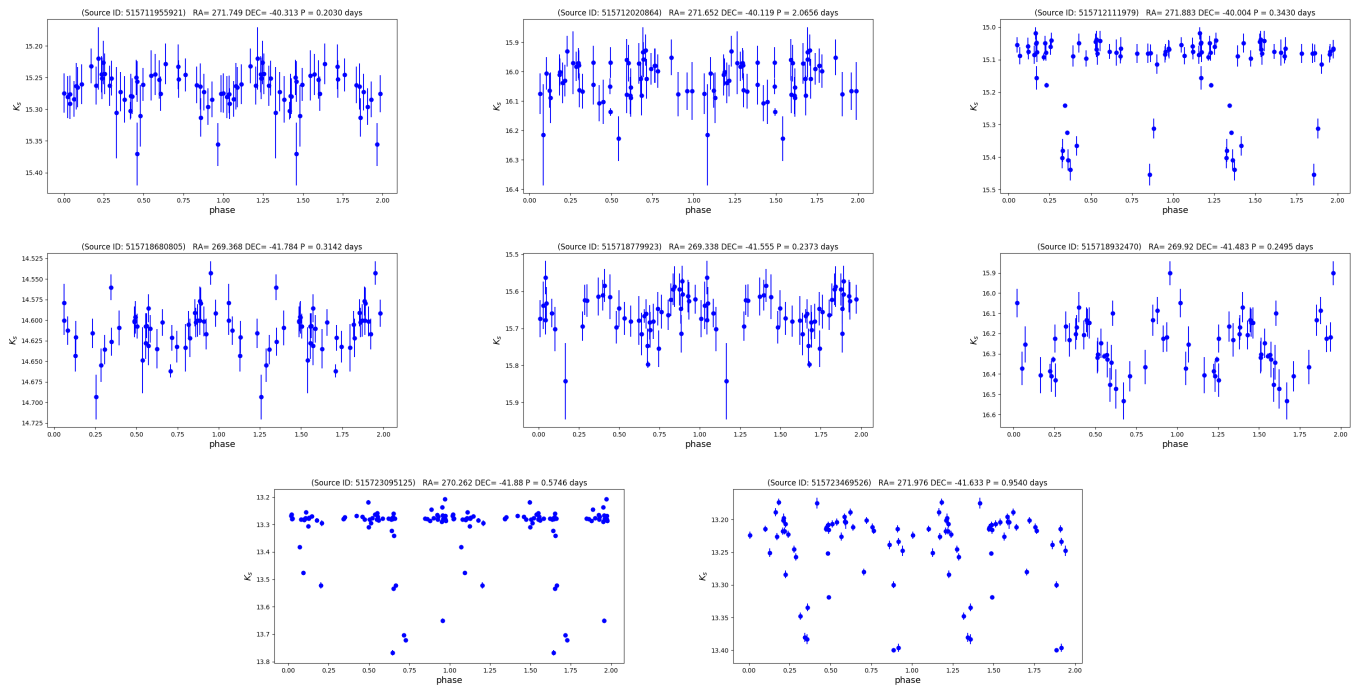


Figure 32. BHB stars light curves corresponding to 2^{nd} category eclipsing binaries.